Lipid nanoparticle technology for mRNA delivery: bridging vaccine applications with fundamental insights into nano-bio interactions

Escalona Rayo, O.

Chapter 2

In vitro and *in vivo* evaluation of clinically-approved ionizable cationic lipids shows divergent results between mRNA transfection and vaccine efficacy

Ionizable cationic lipids (ICLs) play an essential role in the effectiveness of lipid nanoparticles (LNPs) for the delivery of mRNA-based vaccines and therapeutics; therefore, critical evaluations of their biological performance would extend the existing knowledge in the field. In the present Chapter, we examined the effects of three clinically-approved ICLs, Dlin-MC3-DMA, ALC-0315 and SM-102, as well as DODAP, on the *in vitro* and *in vivo* performance of LNPs for mRNA delivery and vaccine efficacy. mRNA-LNPs containing these lipids were successfully prepared, which were all found to be very similar in their physicochemical properties and mRNA encapsulation efficiencies. Furthermore, the results of the *in vitro* studies indicated that these mRNA-LNPs were efficiently taken up by immortalized and primary immune cells with comparable efficiency; however, SM-102-based LNPs were superior in inducing protein expression and antigen-specific T cell proliferation. In contrast, *in vivo* studies revealed that LNPs containing ALC-0315 and SM-102 yielded almost identical protein expression levels in zebrafish embryos, which were significantly higher than Dlin-MC3-DMA-based LNPs. Additionally, a mouse immunization study demonstrated that a single-dose subcutaneous administration of the mRNA-LNPs resulted in a high production of intracellular cytokines by antigen-specific T cells, but no significant differences among the three clinically-approved ICLs were observed, suggesting a weak correlation between *in vitro* and *in vivo* outcomes. This Chapter provides strong evidence that ICLs modulate the performance of mRNA-LNPs and that *in vitro* data do not adequately predict their *in vivo* behavior.

This chapter was published as a research article: O. Escalona-Rayo, Y. Zeng, R.A. Knol, T.J.F. Kock, D. Aschmann, B. Slütter, A. Kros. Biomed Pharmacother 2023;165:115065.

1. Introduction

The development of mRNA-based therapeutics and vaccines has revolutionized the landscape of medicine in the past few years as administration of exogenous mRNA allows to produce any protein of interest, such as antigens, inside the cells [1–3]. A perfect example of this is the prompt and successful development of the two mRNA-based vaccines against SARS-CoV-19 to combat the COVID-19 pandemic [4,5]. Due to its unstable nature and inability to cross biological membranes, mRNA is generally encapsulated into nanoparticle delivery systems [6,7]. In this context, lipid nanoparticles (LNPs) are the leading non-viral vector platform for safe and effective mRNA delivery as they are able to protect mRNA against nuclease degradation, avoid immune detection, reach the target cells, promote cellular entry, facilitate endosomal escape, and release mRNA into the cytosol where it is translated into the protein of interest [2,8,9]. To date, there are only a few RNA-LNP products that have been approved by the US Food and Drug Administration (FDA) and European Medicines Agency (EMA) for clinical use—e.g., Patisiran (Onpattro®), a siRNA-LNP formulation for liver-based gene silencing, and the two mRNA-LNP COVID-19 vaccines (BNT162b2-Comirnaty® and mRNA-1273-Spikevax®) [10–12]. The lipid composition of these RNA-LNP formulations consists of four components: an ionizable cationic lipid (ICL), cholesterol, a phospholipid (1,2-distearoyl-sn-glycero-3-phosphocholine, DSPC), and a polyethylene glycol (PEG)-lipid conjugate [11–13]. These lipid components are essential for LNP formation and stability as well as mRNA efficacy [13].

The success of LNPs for mRNA delivery mainly relies on the ICL, and its features—pK_a (the negative base-10 logarithm of the acid dissociation constant) and molecular shape—dictate the *in vitro* and *in vivo* performance of mRNA-LNPs [14,15]. ICLs are a class of pH-sensitive lipids that contain, at least, a tertiary amine that is in its non-ionized form (neutral) at physiological pH (7.4), but when the pH is lower than its pK_a, it gets protonated and thus positively charged. Compared to permanent cationic lipids, ICLs (neutral form) show fewer interactions with blood cells and lower immune-activation potency, which make LNPs more biocompatible and less immunogenic [8,16]. On the other hand, efficient mRNA encapsulation into LNPs is achieved at acidic pH (~4.0), in which the ICL is positively charged to complex anionic RNA molecules [6,7]. In addition, ICLs promote endosomal escape after endocytosis-mediated cellular internalization of LNPs. The acidic nature of the endosomal environment (pH < 6.5) leads to protonation of the ICLs that interact with anionic endosomal phospholipids

forming cone-shaped ion pairs, which results in endosomal membrane disruption and subsequent mRNA release to the cytosol [8,15,17]. The molecular shape of the ICLs also contributes to the endosomal escape of LNPs. ICLs with cone-shaped morphology—head group cross-sectional area smaller than the lipid tail region—likely form inverted hexagonal phases with anionic endosomal phospholipids that can destabilize the endosomal membrane and thus release the mRNA cargo to the cytosol [18–20]. In this sense, the ICLs in the clinically-approved RNA-LNP products, Dlin-MC3-DMA (Onpattro®), ALC-0315 (BNT162b2-Comirnaty®) and SM-102 (mRNA-1273-Spikevax®), were designed to display an apparent pK_a value in the range of 6.1 – 6.7, as well as a markedly cone-shape morphology [14,20]. With the growing evidence that the therapeutic and vaccine efficacy of LNPs is directly related to the ICL properties, full characterization and evaluation of their *in vitro* and *in vivo* performance are of the utmost importance, since discrepancies between *in vitro* and *in vivo* observations are commonly reported [21,22]. Regarding the clinically-approved ICLs, Ferraresso et al., recently reported the comparison of Dlin-MC3-DMA and ALC-0315 for LNP-mediated siRNA delivery to hepatocytes and hepatic stellate cells in mice, and they found that ALC-0315-based LNPs displayed a higher *in vivo* knockdown of target proteins in comparison to LNPs containing Dlin-MC3-DMA, but the latter exhibited lower liver toxicity [23]. Another study showed that, after intramuscular administration, mRNA-LNPs with SM-102 were more effective than Dlin-MC3-DMA in inducing antibody production, as well as displaying enhanced biodegradability, leading to an improved tolerability [24]. However, to our knowledge, we are the first to report the direct comparison of the potency and efficacy of Dlin-MC3-DMA, ALC-0315 and SM-102 in terms of *in vitro* and *in in vivo* mRNA transfection, protein expression, and T-cell activation and expansion.

The focus of our study was to systematically compare the three clinically-approved ICLs, Dlin-MC3-DMA, ALC-0315 and SM-102, in LNPs for their ability to deliver mRNA to immune cells and elicit cellular immune responses. DODAP was also included in this study as it was the first ICL synthesized for nucleic acid delivery [25]. mRNA-LNPs containing these ICLs were prepared by a rapid-mixing method and characterized in terms of particle size and size uniformity, surface charge, morphology, mRNA encapsulation ability and storage stability. mRNA transfection and protein expression efficiencies were investigated both *in vitro* (immortalized and primary immune cells) and *in vivo* (zebrafish embryos). We hypothesized that the distinct ICLs in LNPs would result in differences in T-cell-inducing vaccine efficacy *in vivo*—the study was performed in a mouse model.

2. Results and discussion

2.1. Preparation and characterization of mRNA-LNPs

This study was designed to assess the effects of different ICLs may exert on the LNP physicochemical properties, cellular internalization, mRNA transfection, protein expression and vaccine efficacy. To accomplish this, we selected a set of four ICLs: DODAP, Dlin-MC3-DMA, ALC-0315 and SM-102 (Figure 1a). Using these ICLs, we then prepared LNPs containing either OVA- or EGFP-mRNA (Figure 1b). The lipid composition of LNPs was ICL/cholesterol/DSPC/DMG-PEG2k with mole ratios of 50/38.5/10/1.5, and the N/P lipid:mRNA ratio was 6:1 (Figure 1c).

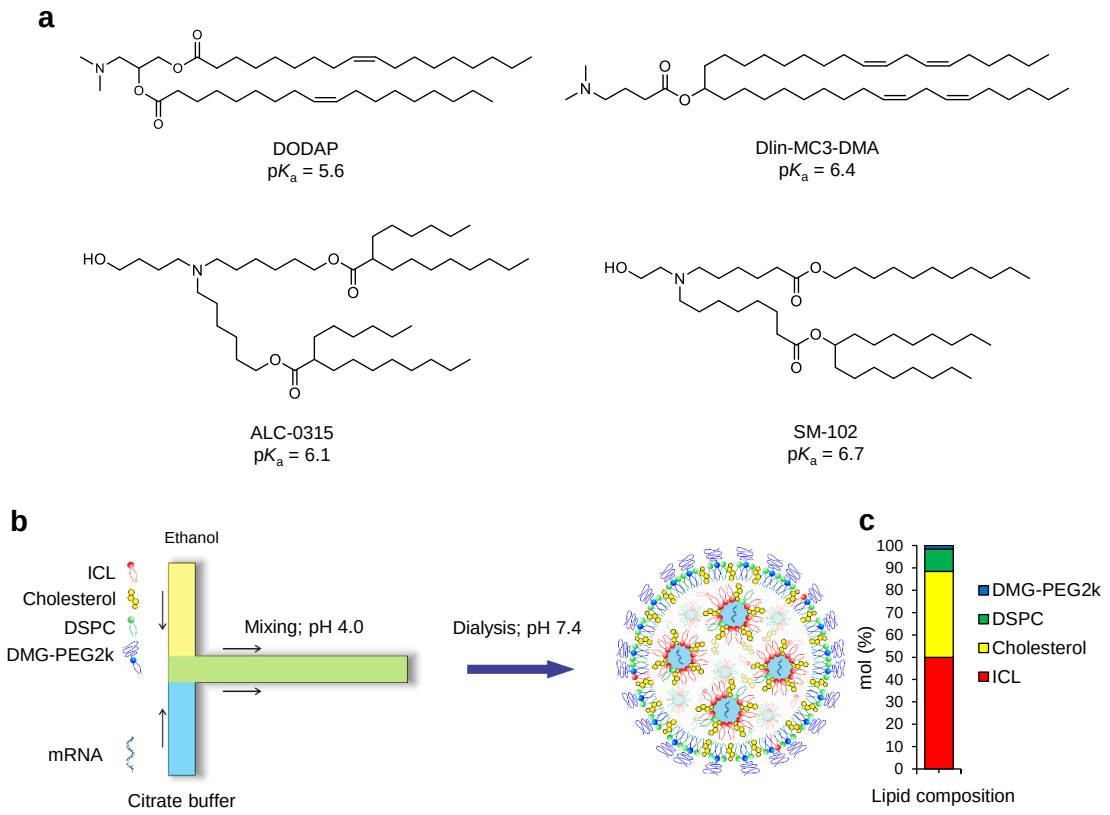

Figure 1. Design and preparation of mRNA-LNPs containing different ICLs. **a** Chemical structure and pK_a of the ICLs used in this work. **b** Schematic representation of LNP preparation using a rapid-mixing platform approach, and **c** Lipid composition of the mRNA-LNPs.

We first checked the physicochemical characteristics of the four OVA-mRNA-LNP formulations. The results given in Table 1 show that these mRNA-LNPs exhibited similar particle size (~100 nm) as well as narrow-size distribution (PDI < 0.2). Furthermore, they had an almost neutral surface charge with zeta potential values of approximately –10 mV, except

for DODAP-based LNPs, which presented a more significant negative zeta potential (–16.1 mV). This small variation could be explained by the degree of ionization of the ICLs and their location in the LNP. On the one hand, a recent study revealed that the ICL (Dlin-MC3-DMA) is located not only in the LNP core but also on the LNP surface [26]. On the other hand, DODAP has an apparent pK_a value of 5.6, which is lower than those corresponding to Dlin-MC3-DMA (pK_a 6.4), ALC-0315 (pK_a 6.1) and SM-102 (pK_a 6.7) [14,20]. According to the Henderson-Hasselbach equation, a lower percentage of ionization of DODAP at pH 7.4 is expected, resulting in a reduced presence of positive charges on the LNP surface. Cryo-EM imaging (Figure 2a) shows that the morphology of the four mRNA-LNPs was spherical with an electron-dense inner core surrounded by a monolayer, as previously reported [26]. Furthermore, the particle size and uniformity in particle size distribution of the LNPs seen by cryo-EM agreed with particle size and PDI determined by DLS. On the other hand, evaluation of encapsulation efficiencies (EE) demonstrated that mRNA was efficiently encapsulated in the LNPs containing Dlin-MC3-DMA, ALC-0315 and SM-102 as the ICLs, reaching an EE higher than 90%, while the EE of DODAP-based LNPs was about 80%. This implies that Dlin-MC3-DMA, ALC-0315 and SM-102 are better ICLs than DODAP for mRNA encapsulation, because of their higher pK_a.

Table 1. Physicochemical properties of the four OVA-mRNA-LNP formulations.

LNPs	Particle size (nm)	PDI	Zeta potential (mV)	EE (%)
DODAP	97.7 ± 1.5	0.148 ± 0.017	–16.10 ± 2.23	83.73 ± 1.72
Dlin-MC3-DMA	103.2 ± 0.8	0.151 ± 0.016	–10.84 ± 1.50	94.78 ± 0.62
ALC-0315	112.3 ± 1.8	0.168 ± 0.014	–11.25 ± 0.68	98.84 ± 1.47
SM-102	102.5 ± 1.0	0.155 ± 0.019	–9.34 ± 1.02	98.96 ± 0.58

Data are shown as mean ± SD of three independent experiments.

Subsequently, we studied the stability of the LNPs over time. Particle size, PDI, zeta potential and mRNA content of the four LNP formulations were measured immediately after preparation and for a period of four weeks after storage at 4 °C. In general, measurements of particle size and PDI of the stored LNPs demonstrated very good stability after 4 weeks; however, the absolute value of zeta potential slightly decreased (Figure 2b-d). In contrast, mRNA content significantly decreased over time, although no discernable difference between the ICL compositions was observed (Figure 2e). These observations are in agreement with

previous works, which demonstrated that LNPs containing either Dlin-MC3-DMA or C12-200 as the ICLs kept their particle size during long-term storage at 4 °C, while a significant drop in the mRNA encapsulation efficiency was observed, which resulted in a reduced mRNA delivery efficiency *in vitro* and *in vivo* [27,28]. The decrease in RNA content may be ascribable to the presence of water in the LNP core that could hydrolyze the mRNA molecules [7]. It has been reported that the water content in Dlin-MC3-DMA-based LNPs is around 24% (volume fraction) [26], and this water content could vary depending on the LNP ultrastructure, which is, in turn, determined by the LNP components [29].

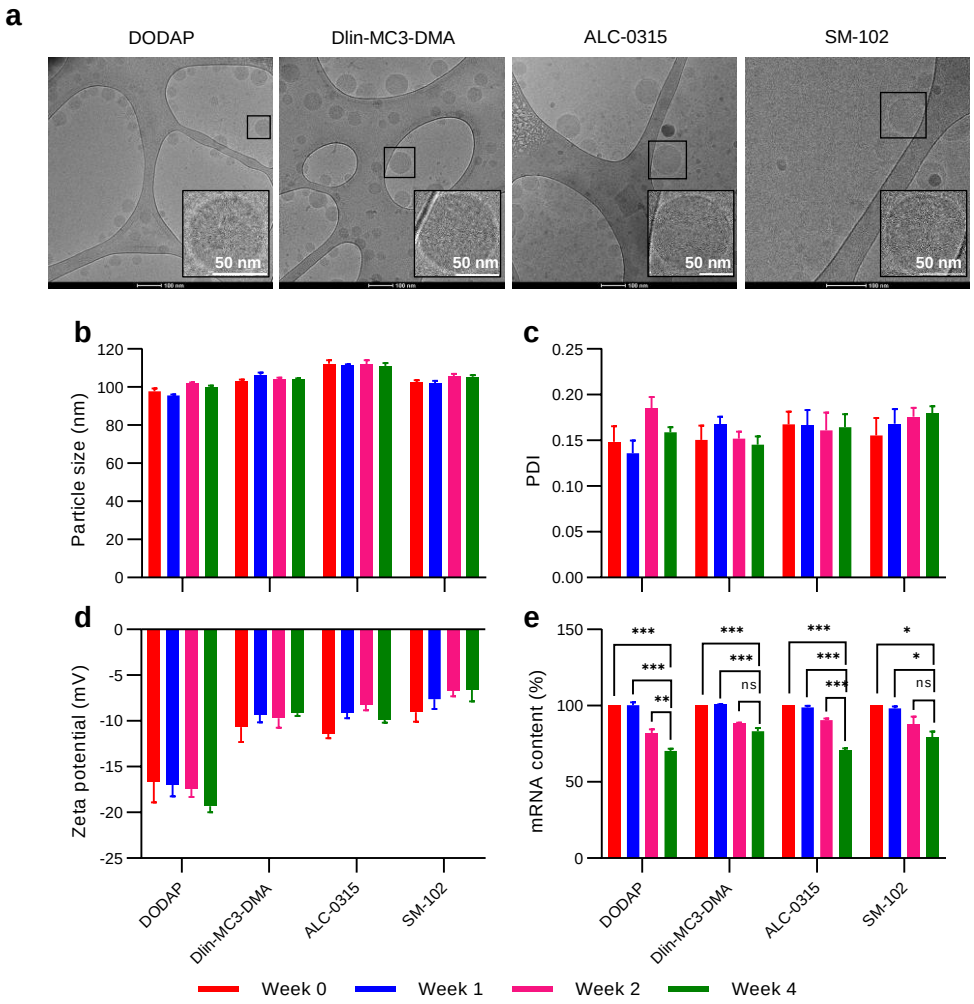

Figure 2. Morphological characterization and storage stability of the mRNA-LNP formulations. **a** Cryo-TEM micrographs of mRNA-LNPs made with the four ICLs (DODAP, Dlin-MC3-DMA, ALC-0315 and SM-102). LNPs show a spherical morphology with a dense inner core enclosed by a monolayer. **b** Particle size, **c** PDI, **d** zeta potential and **e** mRNA content of the four mRNA-LNP formulations at various time intervals during the stability study. Data are shown as mean ± SD, n = 3; *p < 0.05, **p < 0.01 and ***p < 0.001.

All these results suggest that the studied ICLs have a minimal impact on the physicochemical properties of mRNA-LNPs particularly on zeta potential and EE; however, these properties remain stable for at least 4 weeks but not the encapsulated mRNA, probably due to a potential degradation.

2.2. *In vitro* mRNA transfection and translation

Immortalized (dendritic cells, DC2.4, and macrophages, RAW264.7) and primary (BMDCs) immune cells were used to investigate the effect of the four ICLs on cellular internalization and mRNA transfection. First, we evaluated the cytotoxicity of naked OVA-mRNA and OVA-mRNA-LNPs in the cells. In this respect, naked mRNA and the four different LNP formulations were incubated with the cells for 24 h at various mRNA concentrations ranging from 0.01 to 1000 ng mL^{-1}. The results revealed that neither naked mRNA nor mRNA-LNP formulations decreased cell viability more than 20% (Figure S1a-c), which indicates that they all exhibited excellent biocompatibility. To compare the cellular uptake and mRNA transfection of the four ICLs, LNPs were formulated with mRNA encoding EGFP (a fluorescent reporter protein) and labelled with DiD (a fluorescent probe), exposed to cells at four mRNA concentrations (100, 250, 500 and 1000 ng mL^{-1}) for 24 h, followed by flow cytometry and confocal microscopy analysis. We found that the substitution of OVA-mRNA for EGFP-mRNA and incorporation of DiD did not have a substantial impact on the physicochemical properties of the mRNA-LNPs (Table S1). After 24 h of incubation, efficient cellular uptake (>90% DiD^+ cells) of DC2.4 cells, RAW264.7 cells and BMDCs was achieved by all LNP formulations, even at the lowest EGFP-mRNA concentration tested, whereas naked mRNA failed to enter the cells (Figure 3a, Figure S2a, and Figure S3a). However, when looking at the intracellular levels (MFI values) of DiD-mRNA-LNPs, we observed a concentration-dependent uptake with significant differences between the different LNP formulations, particularly, DODAP-based LNPs were less efficient at entering the cells (Figure 3b, Figure S2b, and Figure S3b). LNPs containing Dlin-MC3-DMA, ALC-0315 or SM-102 showed similar cellular uptake behavior. Confocal microscopy images in Figure 3e, Figure S2e and Figure S3e confirmed these observations. The lower cellular uptake efficiency of DODAP-based LNPs could be due to that they exhibited a more negative surface charge than the other ones. Endocytosis is the most important pathway for the cellular internalization of mRNA-LNPs, which has been demonstrated to be dependent on the NP physicochemical properties, including surface charge—more positively charged or less negatively charged NPs are taken up into cells more efficiently than strong negatively charged NPs as they are electrostatically repelled by anionic

phospholipids and proteoglycans present in cell membrane, leading to a poor NP uptake efficiency [30–32].

Next, we evaluated mRNA transfection by monitoring the EGFP expression in the cells. Similar to the cellular uptake trends, we observed a concentration-dependent increase in EGFP expression in the three cell models treated with the EGFP-mRNA-LNPs. The percentages of $EGFP^+$ cells and MFI values increased as the mRNA concentration increased (Figure 3c-d, Figure S2c-d, and Figure S3c-d). Comparison of EGFP expression efficiency ($EGFP^+$ cells and MFI values) revealed the following sequence from high to low: SM-102 > ALC-0315 > Dlin-MC3-DMA > DODAP, regardless of the cell model tested and with SM-102 significantly outperforming all the other ICL ($p<0.001$). No protein expression was detected when naked mRNA was used. Cytosolic mRNA delivery is directly related to the ability of LNPs to escape from endosomes. It has been found that, after endocytosis, ICLs with excellent transfection efficiencies such as Dlin-MC3-DMA or ACU5 (an ALC-0315 analog) predominately accumulate in the early and recycling endosomes, while less efficient ICLs do in the late endosome and/or lysosome [33]. The early and recycling endosomes have an intraluminal pH around 6.0-6.5, in which Dlin-MC3-DMA (pK_a 6.4), ALC-0315 (pK_a 6.1) and SM-102 (pK_a 6.7) are expected to be positively charged and interact with anionic phospholipids present in the endosomal membrane to form cone-shaped ion pairs, leading to membrane fusion/disruption and subsequent endosomal escape [17–20,34]. Indeed, the degree of ionization could be one of the reasons why SM-102 exhibited the highest mRNA transfection efficiency and DODAP failed to produce significant levels of EGFP—DODAP-based LNPs have an apparent pK_a of 5.64, which is too low for protonation in the early and recycling endosomes [13,17,20]. Furthermore, Dlin-MC3-DMA, ALC-0315 and SM-102 display a more accentuated coned-shape molecular structure than DODAP, which has been found to be incompatible with the lipid bilayer of cell membranes [18,19,24,35,36]. Additionally, it has been reported that LNPs with a more homogeneous ultrastructure (exterior bilayer and amorphous electron-dense core) such as Dlin-MC3-DMA-based LNPs display a higher *in vitro* and *in vivo* mRNA transfection efficiency than LNPs (DODAP-based LNPs) with heterogeneous ultrastructural features [26,37].

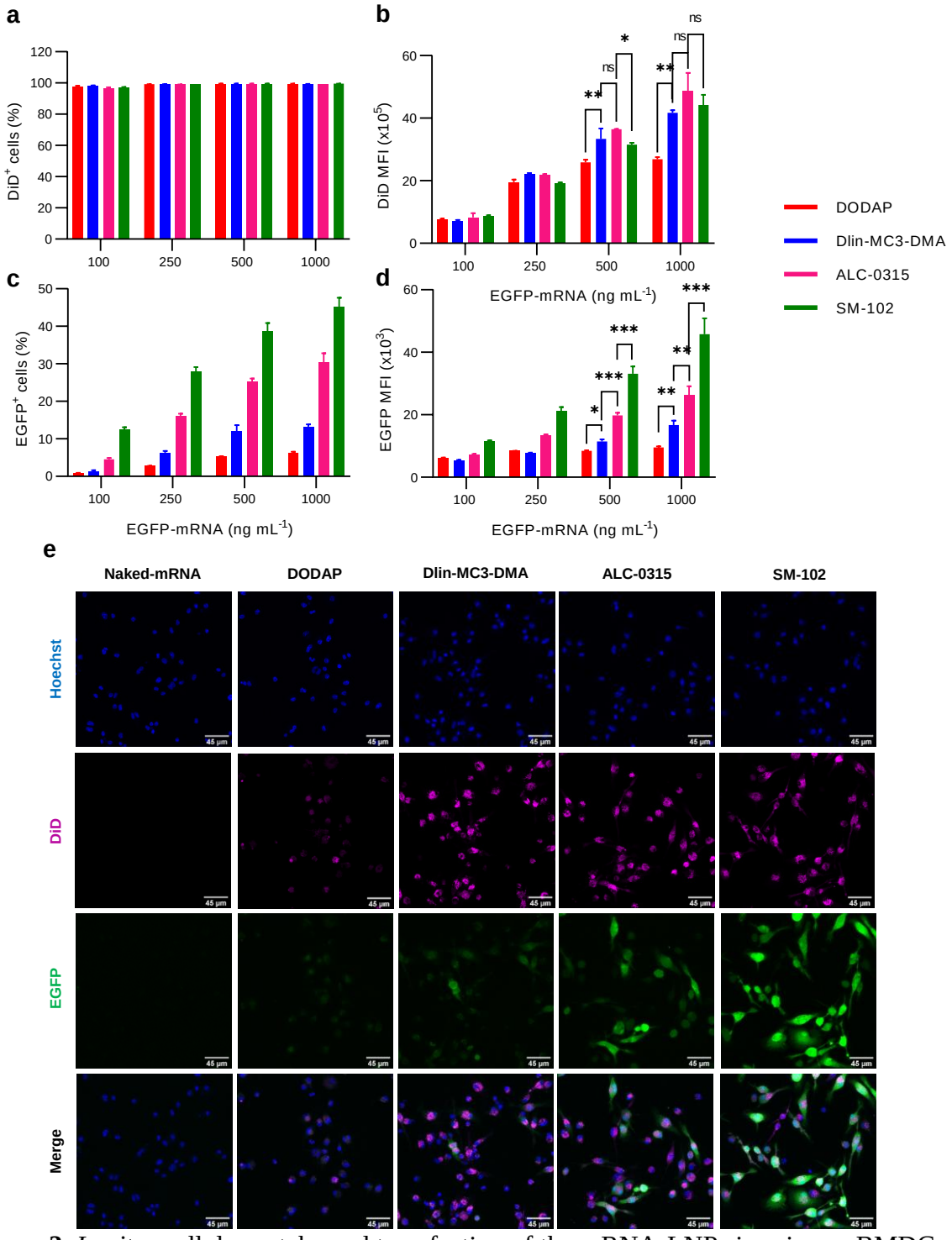

Figure 3. *In vitro* cellular uptake and transfection of the mRNA-LNPs in primary BMDCs. **a-b** Cellular uptake and **c-d** EGFP expression after exposing BMDCs with DiD-labeled EGFP-mRNA-LNPs at different EGFP-mRNA concentrations for 24 h, as determined by flow cytometry. Cellular uptake and EGFP expression efficiencies were influenced by the type of ICL, resulting in the following order: SM-102 > ALC-0315 > Dlin-MC3-DMA > DODAP. **e** Confocal microscopy images of BMDCs showing cellular uptake (magenta; DiD-labeled LNPs) and protein expression (green; EGFP) after 24 h of incubation. The Nucleus was stained with Hoechst (blue). Data are shown as mean ± SD, n = 3; *p < 0.05, **p < 0.01 and ***p < 0.001.

These findings demonstrate that mRNA-LNPs were successfully internalized by immortalized and primary immune cells and that the ICL properties (pK_a and molecular shape) do play an important role in the cellular uptake and endosomal escape of mRNA-LNPs, which are crucial processes in mRNA-mediated protein expression in cells.

2.3. *In vitro* DC activation and *ex vivo* T cell proliferation

Vaccination is one of the major application fields for mRNA-LNPs; hence, we investigated the ability of the four LNP formulations to induce DC activation and proliferation of antigen-specific T cells, which are key processes in vaccine-elicited adaptive immune responses [1,2]. The set of LNPs containing OVA-mRNA (mRNA encoding ovalbumin, an antigen model) were prepared and incubated with BMDCs for 24 h to assess the expression of surface markers (CD40, CD86 and MHC-II), which are indicative of DC activation and maturation [38]. The TLR4 agonist lipopolysaccharide (LPS) was included in the study as a known activator of antigen-presenting cells (APCs) [39]. As reported in Figure 4a, treatment of BMDCs with LPS and LNP formulations (except for DODAP-based LNPs) significantly up-regulated the cell surface expression of CD86. Flow cytometry data analysis revealed significantly higher CD86 levels with SM-102 treatment when compared to LPS, but comparable to ALC-0315. Both ALC-0315 and SM-102, were more effective in up-regulating CD86 expression than Dlin-MC3-DMA. PBS, naked OVA-mRNA and DODAP did not induce any CD86 expression. Regarding CD40 and MHC-II, BMDCs pulsed with LPS overexpressed these two surface markers. In contrast, there was no significant difference in CD40 and MHC-II expression between any of the LNP formulations and PBS, suggesting LNPs did not induce expression of CD40 and MHC-II. It has been demonstrated that stimulation and expansion of T cells can occur through interaction with antigen-loaded MHC-bearing APCs and co-stimulation of CD80/CD86 rather than CD40 [40–42]. In addition, ICLs that induce little co-stimulation may promote tolerance as the absence of CD80/CD86 or CD40 has been shown to increase the sensitivity of T cells to tolerance induction [40]. Therefore, we next assessed whether the four LNP formulations can induce the proliferation of antigen-specific T cells and whether the proliferation efficacy is influenced by the different ICLs. We pulsed BMDCs with naked OVA-mRNA and all four LNP formulations at different OVA-mRNA concentrations (0.02–200 ng mL^{-1}) for 4 h; after that, BMDCs were co-cultured with $CD8^+$ T cells derived from OT-I transgenic mice for 72 h (Figure 4b).

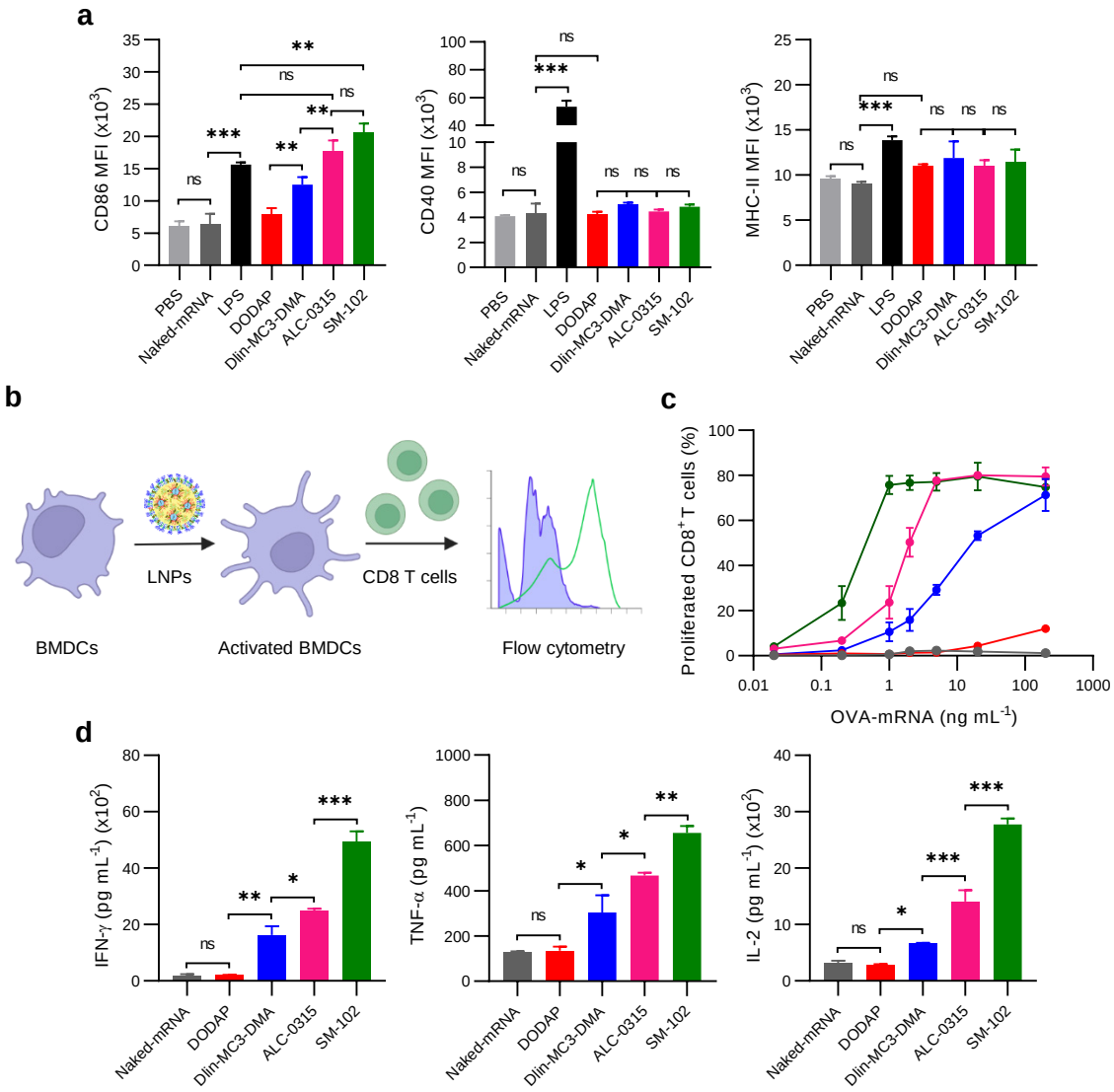

Figure 4. *Ex vivo* proliferation of antigen-specific T cells induced by OVA-mRNA-LNPs. **a** Levels of the surface markers; CD86, CD40 and MHC-II in BMDCs after treating with the four OVA-mRNA-LNP formulations (OVA-mRNA concentration; 1 μg mL^{-1}) for 24 h, as determined by flow cytometry. **B** Schematic showing the *ex vivo* assay to evaluate T cell activation and proliferation. **C** Percentages of proliferated OVA-specific CD8$^+$ T cells after co-cultured with the OVA-mRNA-LNP-treated BMDCs for 72 h, and **d** Cytokines levels in the culture supernatant of the stimulated T cells, as determined by flow cytometry and ELISA assay, respectively. Data are shown as mean ± SD, n = 3; *p < 0.05, **p < 0.01 and ***p < 0.001.

The percentages of proliferated CD8$^+$ T cells-mRNA concentration curves of naked OVA-mRNA and LNP formulations are given in Figure 4c. As expected, the exposure of BMDCs to either naked-mRNA or DODAP-based LNPs resulted in little to no proliferation of antigen-specific T cells, due to their poor transfection and protein expression efficiencies previously observed. In contrast, Dlin-MC3-DMA, ALC-0315 and SM-102 remarkably induced

proliferation of OVA-specific CD8+ T cells in a dose-dependent manner, but with differences and patterns consistent with the transfection studies. The EC50 of Dlin-MC3-DMA-, ALC-0315- and SM-102-based LNPs were found to be 7.69, 1.49 and 0.26 ng mL^{-1}, respectively. T cells co-cultured with SM-102-pulsed BMDCs led to ~30- and ~6-fold increase in T-cell proliferation over Dlin-MC3-DMA and ALC-0315, respectively. Additionally, we tested the influence of the LNP formulations over the $CD8^+$ T-cell effector functions by measuring the secreted cytokine (IFN-γ, TNF-α and IL-2) levels in the BMDC-T-cell coculture supernatant. As shown in Figure 4d, stimulated $CD8^+$ T cells with SM-102-pulsed BMDCs produced the highest levels of the three cytokines, followed by ALC-0315 and Dlin-MC3-DMA. There was no significant difference in the secretion levels of IFN-γ, TNF-α and IL-2 between naked OVA-mRNA and DODAP-based LNPs.

Taking together, a high mRNA transfection efficiency combined with the intrinsic ability to promote DC activation and maturation allows SM-102 to be the most effective ICL of the four tested in inducing T cell activation and proliferation.

2.4. *In vivo* mRNA translation in zebrafish embryos

Prior to exploring the ability of OVA-mRNA-LNPs to elicit specific cellular immune responses *in vivo*, we evaluated whether the *in vitro* findings on protein expression could correlate with *in vivo* observations. First, we aimed to gain insight into the fate of our LNPs in a biological system, since biodistribution of nanoparticle delivery systems plays a key role in therapeutic efficacy [9,43]. To do this, the set of LNP formulations labeled with DiD was injected into wild-type zebrafish embryos, and LNP biodistribution was examined by confocal microscopy (Figure 5a,c). We used zebrafish embryos as a reliable *in vivo* model as they have shown to share several features of the anatomy and physiology with their mammalian equivalents; as a result, zebrafish models have been extensively used for assessing toxicity, biodistribution, blood circulation and targeting ability of nanomedicines, including LNPs [44,45]. At 24 h post-injection, we noted that LNPs were cleared from the blood circulation and accumulated in endothelial cells as well as the extravascular space throughout the zebrafish embryo body, as shown in Figure 5c. It is known that PEG-lipids containing short alkyl chains such as DMG-PEG2k accelerate the blood clearance of LNPs, because they shed from LNPs due to their interaction with serum proteins [46–49]. After PEG dissociation, LNPs interact with biomolecules from biological fluids, mainly serum proteins such as apolipoproteins (Apos), being adsorbed on the LNP surface to form the protein corona of which its composition

has been shown to dictate the LNP interactions with tissues and cells [50]. As depicted in Figure 5c, LNPs preferentially accumulated in the tail region, which is rich in macrophages and scavenger endothelial cells (analogous to mammalian liver sinusoidal endothelial cells). This can be explained by the high endocytic capacity of these cells [51]. In addition, the observed largely non-selective accumulation pattern is in accordance with previous zebrafish biodistribution studies regarding near-neutral charged nanoparticles [52,53]. Moreover, accumulation in the extravascular space seemed higher for LNPs containing the clinically-approved ICLs, especially for ALC-0315-based LNPs. This could be due to the fact that the lipid composition of LNPs can significantly influence the protein corona composition and thus, the interaction of LNPs with specific tissues [50,52–54].

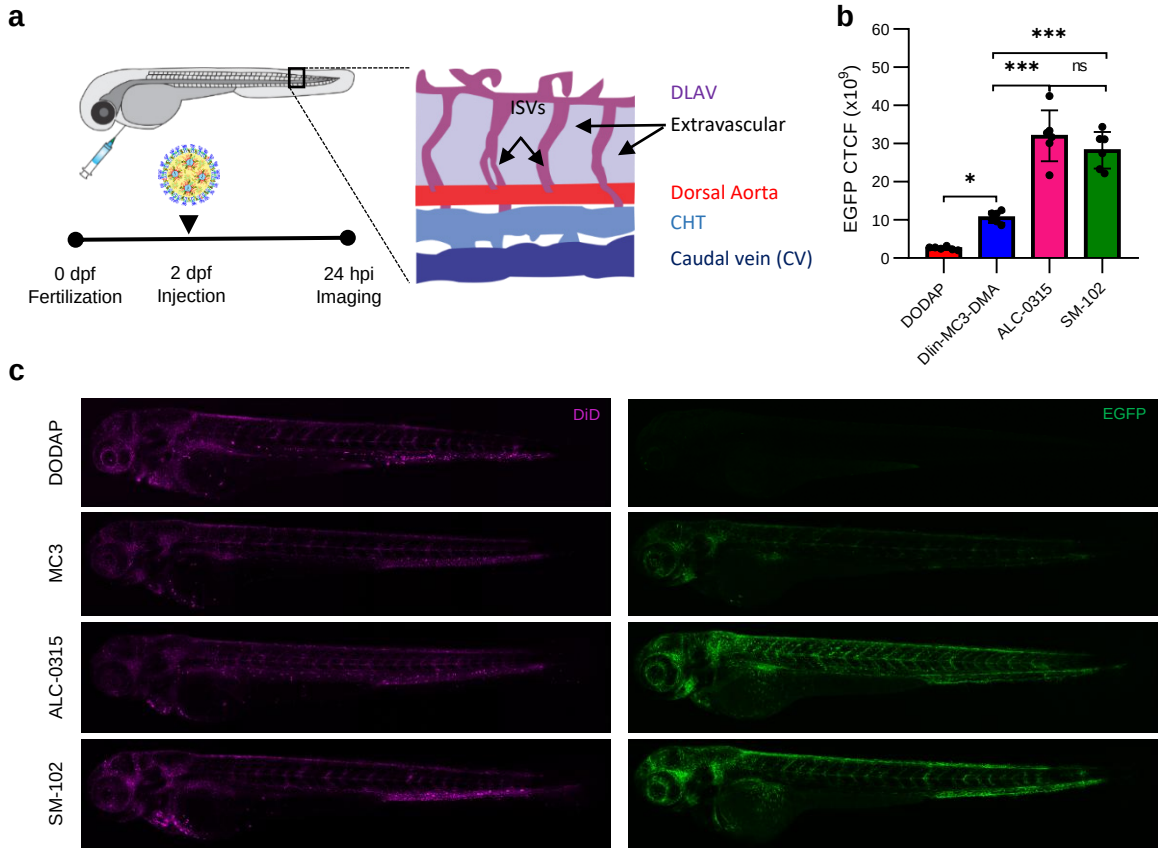

Figure 5. *In vivo* mRNA translation of EGFP-mRNA-LNPs in zebrafish embryos. **a** Schematic illustrating the intravenous injection of the EGFP-mRNA-LNPs in wild-type ABTL zebrafish embryos (2dpf). **b** CTCF fluorescence intensities obtained after injecting the EGFP-mRNA-LNP formulations to zebrafish embryos (EGFP-mRNA dose: 0.3 mg kg^{-1}; injection volume: 1 nL), as determined by confocal microscopy and image analysis. **c** Confocal microscopy images of the zebrafish embryos treated with DODAP, Dlin-MC3-DMA, ALC-0315 or SM-102 in terms of LNP biodistribution (DiD, left) and mRNA transfection (EGFP, right). Data are shown as mean ± SD, n = 6; *p < 0.05, **p < 0.01 and ***p < 0.001.

After the biodistribution study, we investigated the *in vivo* LNP-mediated mRNA translation; therefore, we injected all four EGFP-mRNA LNP formulations into zebrafish embryos (Figure 5a) and EGFP expression was examined by confocal microscopy (Figure 5b-c). In line with the *in vitro* mRNA transfection findings, zebrafish embryo treated with DODAP- and Dlin-MC3-DMA-based LNPs showed a very low and moderate EGFP expression, respectively. Unexpectedly, ALC-0315 and SM-102 exhibited similar protein expression *in vivo*, despite SM-102 displaying a marked superiority for mRNA transfection and translation *in vitro*. The order of *in vivo* protein expression efficiency was found as follows: SM-102 = ALC-0315 > Dlin-MC3-DMA > DODAP. One possible explanation of the observed comparable mRNA translation efficiency between ALC-0315 and SM-102 could be related to the LNP charge-mediated trafficking as surface charge could influence the protein corona composition and subsequent cellular uptake [13]. ALC-0315-based LNPs had a slightly more negative surface charge than LNPs containing SM-102. LNPs with slight negative surface charge have shown to be more efficient for *in vitro* transfection, whereas more negative LNPs displayed higher potency after IV administration, probably due to a more efficient Apo-E adsorption and passive targeting, which could be compensating for the lower endosomal escape efficiency of ALC-0315 compared to SM-102 [20,55].

In summary, the mRNA translation results revealed discrepancies between *in vitro* and *in vivo* performance of the ICLs, particularly, ALC-0315 and SM-102. The latter exhibited superior *in vitro* potency compared to ALC-0315, but both showed similar *in vivo* performance.

2.5. *In vivo* cellular immune response in mice

To test and compare the *in vivo* vaccine efficacy to induce cellular immune responses, the set of OVA-mRNA-LNPs was administered subcutaneously or intravenously as a single injection to C57Bl/6 mice at a dose of 0.25 mg kg^{-1}. At 7 days post-immunization, single-cell suspensions obtained from spleens (splenocytes) were re-stimulated with either PBS or $OVA_{257-264}$ peptide and analyzed by flow cytometry to measure the intracellular cytokine production mediated by OVA-specific T cells (Figure 6a). After *ex vivo* re-stimulation, in comparison to treatment with either naked OVA-mRNA or DODAP, Dlin-MC3-DMA, ALC-0315 and SM-102 led to a significantly higher IFN-γ and IL-2 production (Figure 6b,c). We found that subcutaneous immunization of mice with these LNPs resulted in approximately 3–6% and 2–3% of IFN-γ– and IL-2–producing $CD8^+$ T cells, respectively, suggesting that these OVA-mRNA LNPs triggered a specific immune response to $OVA_{257-264}$ peptide. In contrast, when

these OVA-mRNA LNPs were intravenously administered, no cytokine production was observed (Figure S4a-b), probably due to that mRNA-LNPs, after intravenous administration, lead to particle accumulation and protein expression mainly in the liver [56]. On the other hand, subcutaneously administered LNPs largely remained at the injection site where mRNA is translated into corresponding protein although protein expression has been also observed to occur in the local axial and brachial draining lymph nodes [57,58]. This suggests a cell-mediated transport to the lymph nodes as subcutaneously administered liposomes showed to target cells under the skin, including APCs, which can take up and transport cutaneous antigens to draining local lymph nodes and present them to T cells [59], although further studies are needed to explain the proliferation of antigen-specific T cells detected in the spleen. ALC-0315 and SM-102 showed comparable percentages of IFN-γ– and IL-2–producing $CD8^+$ T cells, which is in the line with our findings regarding *in vivo* protein expression studies.

Surprisingly, compared to ALC-0315 and SM-102, we observed no significant differences in OVA-specific CD8+ T-cell-mediated cytokine production when mice were immunized with Dlin-MC3-DMA, despite the lower *in vitro*/*in vivo* mRNA transfection and translation of Dlin-MC3-DMA-based LNPs. These results suggest that, in contrast to our *in vitro* observations where the proliferation of antigen-specific T cells only depends on the expressed antigen levels in APCs, *in vivo* activation of T cell-mediated immunity also requires other immunological events [24,60]. For instance, it has been demonstrated that intramuscularly administered Dlin-MC3-DMA-based LNPs elicit a stronger innate immune response than SM-102-based LNPs [24,61], which may compensate for the lower transfection efficacy of Dlin-MC3-DMA-based LNPs. Moreover, the effect of the LNP composition on the migration of antigen-loaded mature APCs to the draining lymph nodes—regarding the number of migrating cells—could also explain the observed differences in the *in vivo* activation of antigen-specific T cells [62]; however, further investigation is required. On the other hand, the uptake of mRNA-LNPs is not APC-specific, and neighboring cells can also take them up. Davies et al. demonstrated that mRNA-LNPs mostly remain at the injection site upon subcutaneous administration, which are preferentially taken up by adipocytes [57]. This non-specific uptake of LNPs by APCs could lead to a variation in vaccine efficacy, where the LNP composition may also play an important role.

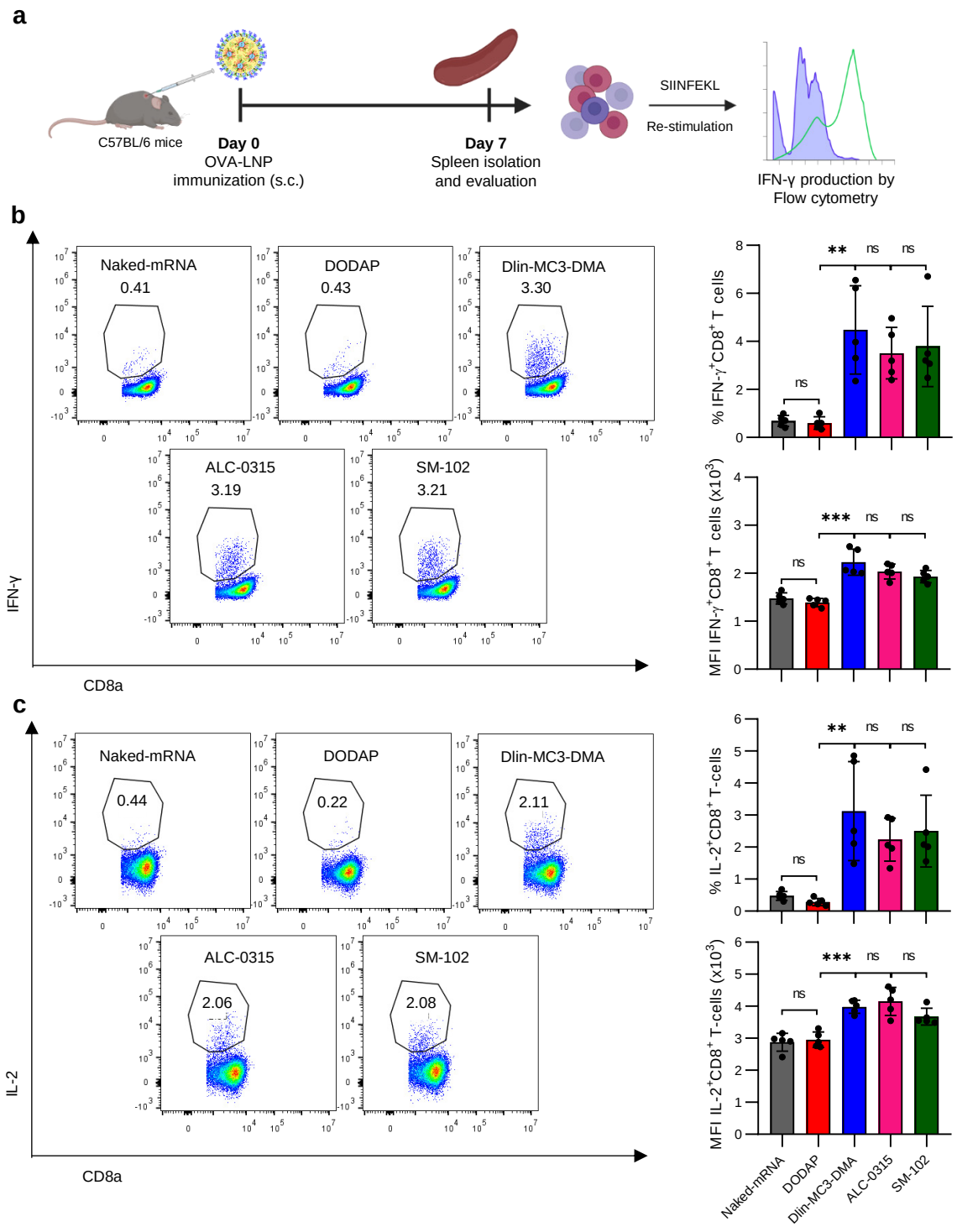

Figure 6. *In vivo* cellular immune response induced by the OVA-mRNA LNPs in mice. **a** Schematic showing the subcutaneous injection of OVA-mRNA-LNPs in C57Bl/6 mice. Percentages of **b** IFN-γ– and **c** IL-2–producing $CD8^+$ T cells after subcutaneous administration of naked OVA-mRNA, DODAP, Dlin-MC3-DMA, ALC-0315 or SM-102 in mice (OVA-mRNA dose: 0.25 mg kg^{-1}), as determined by flow cytometry. Data are shown as mean ± SD, n = 5; *p < 0.05, **p < 0.01 and ***p < 0.001.

All this *in vivo* evidence points towards Dlin-MC3-DMA-, ALC-0315- and SM-102-based LNPs elicited a strong antigen-specific T cell immune response *in vivo* with comparable efficacy.

3. Materials and methods

3.1. Materials

The ICLs: Dlin-MC3-DMA, ALC-0315, and SM-102 were synthesized according to previously reported methods (Supporting Information) [35,63,64]. 1,2-dioleoyl-3-dimethylammonium-propane (18:1 DAP, DODAP), 1,2-distearoyl-sn-glycero-3-phosphocholine (18:0 PC, DSPC), and 1,2-dimyristoyl-rac-glycero-3-methoxypolyethylene glycol-2000 (DMG-PEG2k) were purchased from Avanti Polar Lipids (AL, USA). Cholesterol, lipopolysaccharide (LPS) derived from E. coli strain O111-B4 and Amicon® Ultra-0.5 ml Centrifugal Filter Units (100kDa MWCO) were purchased from Sigma-Aldrich (Zwijndrecht, Netherlands). CleanCap® Ovalbumin mRNA (5-methoxyuridine) (OVA-mRNA) and CleanCap® Enhanced Green Fluorescent Protein mRNA (5-methoxyuridine) (EGFP-mRNA) were supplied by TriLink Biotechnologies through Tebu-Bio (Boechout, Belgium). Penicillin-Streptomycin (PenStrep), L-glutamine (GlutaMAXTM), DiD Solid DiIC18(5) Solid, Quant-itT™ RiboGreen RNA Assay Kit, and Slide-A-Lyzer™ Dialysis Cassettes (20K MWCO, 0.5 mL) were purchased from Thermo Fisher Scientific (Bleiswijk, Netherlands). CD8+ T Cell Isolation Kit was purchased from Miltenyi Biotec (Leiden, Netherlands). Granulocyte-macrophage colony-stimulating factor (GM-CSF) was supplied by Bio-Connect (Huissen, Netherlands). Roswell Park Memorial Institute (RPMI) 1640 medium, Dulbecco's Modified Eagle Medium (DMEM) and Iscove's Modified Dulbecco's Medium (IMDM) were purchased from Lonza (Verviers, Belgium). Fluorescent-conjugated antibodies for flow cytometry were purchased from BioLegend (CA, USA) or Invitrogen (MA, USA). All other reagents were purchased from Sigma-Aldrich.

3.2. Animal and cell culture

Wild-type C57Bl/6 and OT-I transgenic mice were purchased from Jackson Laboratory (CA, USA), bred in-house, kept under standard laboratory conditions, and provided with food and water ad libitum. Zebrafish (Danio rerio, strain AB/TL) were maintained and handled according to the guidelines from the Zebrafish Model Organism Database (http://zfin.org). Fertilization was carried out by natural spawning at the beginning of the light period, and eggs were raised at 28.5 °C in egg water (60 µg mL^{-1} Instant Ocean Sea salts).

DC2.4 cells (a mouse dendritic cell line) were kindly supplied by Kenneth Rock, University of Massachusetts Medical School, Worcester, MA, USA. RAW 264.7 cells (a mouse

macrophage cell line) were supplied by ATCC® (VA, USA). DC2.4 and RAW 264.7 cells were cultured in RPMI1640 and DMEM, respectively. Both mediums were supplemented with 10% FCS, 1% PenStrep and 2 mM GlutaMAX^{TM}. Cells were kept humidified at 37 °C with 5% CO_2. Primary bone marrow-derived dendritic cells (BMDCs) were prepared as previously described [65]. In brief, bone marrow progenitor cells were obtained by flushing the murine tibia and femur of six-to-eight-week-old C57BL/6 mice and stimulated for 10 days with 20 ng mL^{-1} GM-CSF in supplemented IMDM medium, which was changed every 2 days, and semi-attached cells were harvested for experiments. $CD8^+$ T cells were isolated from spleens of OT-I mice via magnetic separation, purified according to manufacturer's protocol and stained with carboxyfluorescein succinimidyl ester (CFSE) to monitor cell proliferation [51].

All studies involving experimental animals were conducted in full accordance with the protocols approved by the Ethics Committee for Animal Experiments of Leiden University and adhered to the Dutch government guidelines and the Directive 2010/63/EU of the European Parliament.

3.3. Preparation of mRNA-LNPs

mRNA-LNPs were prepared by a rapid-mixing technique employing a T-junction device as previously described [44]. Briefly, mRNA and lipids were separately dissolved in 50 mM sodium citrate buffer pH 4.0 and ethanol absolute, respectively. For the labeled LNPs, the fluorescent probe (DiD) was incorporated in the ethanolic solution. The two solutions were mixed using syringe pumps and passed through a T-junction mixer. The resulting suspension was dialyzed against phosphate buffered saline (1x PBS) pH 7.4. LNPs were composed of the ICL (DODAP, Dlin-MC3-DMA, ALC-0315, or SM-102)/cholesterol/DSPC/DMG-PEG2k at % mole ratios of 50:38.5:10:1.5, respectively [10,12]. For DiD-LNPs, DiD was used at a concentration of. 0.2%. OVA-mRNA or EGFP-mRNA were encapsulated into LNPs. The N:P ratio (moles amine of the ICL:moles phosphate of mRNA) was set to 6. For particle morphology studies and *in vivo* experiments, LNPs were concentrated after dialysis using the 100 kDA MWCO Amicon® Ultra Centrifugal filters.

3.4. Characterization of mRNA-LNPs

The particle size and polydispersity index (PDI) of the mRNA-LNPs diluted in 1x PBS pH 7.4 were measured by dynamic light scattering (DLS) using Zetasizer Nano-S (Malvern Instruments Ltd., Worcestshire, UK) at 25 °C. Zeta potential was measured by particle

electrophoretic mobility using Zetasizer Nano-ZS (Malvern Instruments Ltd), employing folded capillary zeta potential cells (DTS1070, Malvern)—LNPs were diluted in 0.1x PBS pH 7.4. Concentration and encapsulation of mRNA in LNPs were determined using the Quant-it™ RiboGreen RNA Assay. LNPs were diluted in 1x TE buffer with and without Triton X-100 (to induce the LNP breaking), followed by the addition of the RiboGreen reagent diluted in 1x TE buffer. Standard curves were also prepared. RiboGreen fluorescence was measured using a TECAN Spark® microplate reader (Männedorf, Switzerland). Encapsulation efficiency (EE) was calculated according to the following formula: EE (%) = [(Total mRNA – free mRNA)/Total mRNA] x 100.

The morphology of the LNPs was assessed by cryogenic transmission electron microscopy (cryo-EM) using a Talos L120C (NeCEN, Leiden University) operating at 120 kV. The LNP (3 µL, ~20 mM total lipid concentration) sample was applied to a freshly glow-discharged carbon 200 mesh Cu grid (Lacey carbon film, Electron Microscopy Sciences, Aurion, Wageningen, The Netherlands), then waiting for 3 seconds and lastly the excess liquid was blotted off for 3 seconds and plunge-frozen in liquid ethane using a Vitrobot plunge-freezer (FEI VitrobotTM Mark III, Thermo Fisher Scientific, Waltham, MA, USA), which was kept at 100% humidity during the whole procedure. Images were recorded on a BM-Ceta (4k x 4k) at a nominal magnification of 45000x or 73000x (2.19 or 1.34 Ångstrom per pixel) and defocus of -5.0 µm.

3.5. Stability of mRNA-LNPs

The storage stability of the mRNA-LNPs was performed at 4 °C for 4 weeks. LNP samples were withdrawn at different times (0, 1, 2, and 4 weeks) and analyzed for changes in particle size, PDI, zeta potential, and mRNA content.

3.6. Cell viability

DC2.4, RAW264.7 or BMDCs were seeded in 96-well plates at a density of 2 x 10^4 viable cells/well and allowed to attach for 24 h at 37 °C. The cells were treated with either naked mRNA or the mRNA-LNP formulations at different mRNA concentrations (0.01–1000 ng mL^{-1}). After 24 h of incubation, cells were washed with PBS, and cell viability was determined by alamarBlue™ (Thermo Fisher Scientific) cell viability assay (DC2.4 and RAW264.7) or flow cytometry, APC-eFluor780, (BMDCs). Untreated cells were taken as control with 100% viability.

3.7. *In vitro* mRNA transfection and translation

The mRNA transfection and translation studies were performed using EGFP-mRNA-LNPs labeled with DiD. Briefly, Cells—DC2.4, RAW264.7 and BMDCs—were seeded at a density of 2 x 10^4 cells/well in a 96-well plate and allowed to adhere for 24 h. Then, cells were treated with different concentrations (100, 250, 500, and 1000 ng mL^{-1}) of either naked EGFP-mRNA or the equivalent concentration of EGFP-mRNA-LNPs in supplemented medium and incubated for 24 h at 37 °C in a 5% CO_2 atmosphere. After incubation, cells were washed with PBS, resuspended in FACS buffer (PBS, 2% FBS, 0.1% sodium azide and 1mM EDTA) and analyzed by flow cytometry (CytoFLEX S, Beckman Coulter, CA, USA) for DiD and EGFP fluorescence. Data were analyzed using FlowJo software V10 (Tree Star Inc., OR, USA). The percentages of positive cells (DiD^+ and $EGFP^+$ cells) as well as the mean fluorescence intensity (MFI) values of the positive cells were reported.

For imaging, the cells were seeded in 8-well plate (2 x 10^4 cells/well) and incubated at 37 °C for 24 h. Then, they were treated with naked EGFP-mRNA and DiD-labeled EGFP-mRNA-LNPs at a mRNA concentration of 1 µg mL^{-1} and incubated for 24 h. After treatment, cells were washed with PBS, treated with Hoechst 33342 for nuclear staining and fixed with 4% paraformaldehyde, followed by confocal microscopy imaging (Leica TCS SP8 confocal laser scanning microscope, Leica microsystems, Wetzlar, Germany). Images were processed using ImageJ® software (United States National Institutes of Health, MD, USA).

3.8. *In vitro* DC activation

Immature BMDCs were stimulated with PBS, LPS, naked OVA-mRNA and OVA-mRNA-LNPs at an OVA-mRNA concentration of 1 µg mL^{-1} for 24 h in supplemented medium. After that, cells were washed and stained for CD11c (FITC), CD40 (PE), CD86 (APC), MHC-II (eFluor450) and viability (APC-eFluor780). Expression of surface markers was analyzed by flow cytometry. Data were analyzed with FlowJo software V10.

3.9. *Ex vivo* expansion of antigen-specific T cells

Evaluation of the *ex vivo* proliferation of antigen-specific T cells was carried as previously described [51]. In brief, BMDCs (2 x 10^4 cells/well) were exposed to naked OVA-mRNA and the four OVA-mRNA-LNP formulations at different OVA-mRNA concentrations (0.2–200 ng mL^{-1}) for 4 h. Subsequently, the BMDCs were washed with PBS and co-cultured with CD8 T cells (6 x 10^4 cells/well) for 72 h in supplemented RPMI. After incubation, cells were washed

and stained for Thy1.2 (PeCy7), CD8 (efluor450), CD25 (APC) and viability (APC-eFluor780). The cells were washed with PBS, resuspended in FACS buffer and analyzed by flow cytometry. Data were analyzed with FlowJo software V10. Levels of cytokines (INF-γ, TNF-α and IL-2) in the supernatants (at mRNA concentration of 2 ng mL^{-1}) of BMDC-T cell cocultures were measured by an enzyme-linked immunosorbent assay (ELISA), following the protocol described in [51].

3.10. *In vivo* mRNA translation in zebrafish embryos

Biodistribution and mRNA translation studies were conducted on wild-type AB/TL zebrafish embryos. Before microinjection, embryos were embedded and anesthetized in 0.4% agarose gel in egg water (60 µg mL^{-1} Instant Ocean Sea salts) containing 0.01% tricaine. Zebrafish embryos at 2-days post fertilization (dpf) were injected via common cardinal vein with the DiD-labeled EGFP-mRNA-LNP formulations at a mRNA dose of 0.3 mg kg^{-1}. At 24 h post-injection, DiD-labeled LNPs and EGFP expression were examined for 6 whole embryos per group by confocal microscopy, and images were processed and analyzed using ImageJ® software to calculate of the corrected total cell fluorescence (CTCF) by using the following formula: CTCF = integrated density – (area of total fish x mean fluorescence of the background reading). Calculation of CTCF allowed for the comparison between groups.

3.11. *In vivo* antigen-specific T-cell response

To determine the antigen-specific T-cell response of the mRNA-LNPs, C57Bl/6 mice (n = 5 for each group) were injected subcutaneously or intravenously with the OVA-mRNA LNPs at an OVA-mRNA dose of 0.25 mg kg^{-1}. After seven days, mice were sacrificed by cervical dislocation, and the spleen was removed. Spleens were harvested and mechanically processed with a 70-µm cell strainer to produce a single-cell suspension. After centrifugation of the single-cell suspension (spleen suspension), the supernatant was discarded, and ammonium-chloride-potassium (ACK) lysing buffer was added to the pellet to lyse red blood cells. The resulting suspension was diluted with PBS and then, centrifuged to obtain the cell pellet (splenocytes), which was resuspended in RPMI1640 medium. The obtained splenocytes were stimulated for 4 h at 37 °C with either PBS or OVA257-264 peptide in the presence of Brefeldin A. After stimulation, cells were washed and stained for surface markers—αThy1.2 (PE-cy7), αCD8α (BV510) and viability (Fixable Live/Dead marker, APC-eFluor780). To measure cytokine production, splenocytes were then washed with PBS, fixed and permeabilized with BD Cytofix/Cytoperm buffer and stained for intracellular cytokines—αIFN-γ (VB650) and αIL-2

(APC). Finally, the cells were washed and resuspended in FACS buffer to be analyzed by flow cytometry. Data were analyzed with FlowJo software V10. The percentages of cytokine^{+}CD8^{+} T cells) and MFI values of this cell population were reported.

3.12. Statistical analysis

Quantitative data were expressed as mean ± standard deviation (SD). Data were processed and analyzed with GraphPad Prism® (Version 8.00, GraphPad Software, Inc., CA, USA). One-way ANOVA followed by Tukey's honestly significant difference test was applied to compare groups. Data were considered as statistically significant for values of $p < 0.05$ (*$p < 0.05$, **$p < 0.01$ and ***$p < 0.001$).

4. Supporting information for:

In vitro and *in vivo* evaluation of clinically-approved ionizable cationic lipids shows divergent results between mRNA transfection and vaccine efficacy

4.1. Synthesis of the ICLs

The synthesis of Dlin-MC3-DMA, ALC-0315 and SM-102 was carried out as previously reported [35,63,64].

4.1.2. Synthesis of Dlin-MC3-DMA

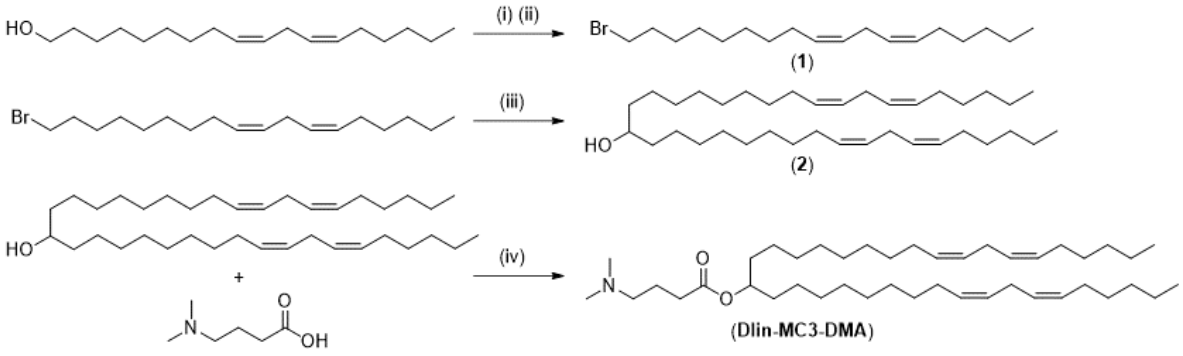

(i) MsCl, NEt_3, DCM; (ii) MgBr.Et_2O, Et_2O; (iii) a) Mg, Et_2O, HCOOEt, NaOMe; (iv) EDCI, DIPEA, DMAP, DCM

Synthesis of 18-bromo-octadeca-6, 9-diene (compound 1).

The fatty alcohol cis,cis-9,12-octadecadien-1-ol (2.6 g, 10 mmol) and triethylamine (1.3 g, 13 mmol) were dissolved in dichloromethane (50 mL) and cooled to 0 °C. Then, a solution of mesyl chloride (1.3 g, 11 mmol) in dichloromethane (20 mL) was slowly added dropwise, and the resulting mixture was gradually warmed to room temperature and stirred overnight. After that, the reaction mixture was diluted with dichloromethane and washed with water (100 mL), saturated $NaHCO_3$ (aq.) (100 mL) and brine (100 mL). The organic phase was then dried over anhydrous $MgSO_4$, filtered and dried under reduced pressure to obtain the mesylate crude product, which was used without further purification. A solution of the resulting mesylate (1.5 g) in anhydrous ether (50 mL) was treated with magnesium bromide ethyl etherate (3.1 g, 11.8 mmol) and refluxed under a nitrogen atmosphere for 24 h. Then, the reaction mixture was diluted with ether and treated with ice-cold water. The organic layer was washed with an 1% aqueous solution of K_2CO_3 (100 mL), brine (100 mL) and dried over anhydrous $MgSO_4$, filtered and dried under reduced pressure to obtain the crude product, which was purified by flash column chromatography (silica gel, 0-1% diethyl ether in hexanes) to yield 0.9 g (60%) of compound 1 as colorless oil.

^{1}H NMR (400 MHz, $CDCl_3$) δ: ppm 5.43 – 5.28 (m, 4H), 3.41 (t, *J* = 6.8 MHz, 2H), 2.77 (t, *J* = 6.8 MHz, 2H), 2.05 (q, *J* = 6.9 MHz, 4H), 1.85 (qt, *J* = 7.0 MHz, 2H), 1.48 – 1.23 (m, 16H), 0.89 (t, *J* = 6.8 MHz, 3H).

^{13}C NMR (101 MHz, CDCl3) δ: ppm 130.38, 130.22, 128.20, 128.06, 34.21, 32.99, 31.71, 29.78, 29.52, 29.50, 29.35, 28.91, 28.34, 27.38, 27.36, 25.80, 22.75, 14.26.

Synthesis of (6Z,9Z,28Z,31Z)-heptatriaconta-6,9,28,31-tetraen-19-ol (Compound 2).

Activated magnesium turnings were put into flame dried, 20-mL, 3-necked, round-bottomed flask equipped with an addition funnel, reflux condenser, rubber septum with nitrogen inlet, and a magnetic stirring bar. A solution of compound 1 (0.5 g, 1.52 mmol) in anhydrous ether (5 mL) was put into the addition funnel, and 5 mL of this solution was slowly added dropwise to the flask under vigorous stirring to initiate the reaction (exothermic reaction), which was confirmed by adding iodine (decolorization of iodine indicates the formation of the Grignard reagent). Once the reaction was initiated, the rest of the compound 1 solution was slowly added dropwise, keeping the reaction under reflux. After adding the compound 1 solution, the reaction was maintained at 35 °C for 2 h and subsequently cooled in an ice bath. After that, a solution of ethyl formate (0.6 g, 0.8 mmol) in anhydrous ether (4 mL) was added as stream to the reaction mixture via the addition funnel, and the reaction mixture was stirred at room temperature for 2h, after which time it was quenched with acetone (10 mL) followed by cold water (60 mL), treated with 300 mL of a 10% aqueous solution of H_2SO_4 and extracted with ether (3 x 100 mL). The combined organic layers were dried over anhydrous $MgSO_4$, filtered and dried under reduced pressure to obtain the crude product, which was then treated with a solution of sodium (1 g) in methanol (200 mL) at room temperature overnight. The resulting reaction mixture was treated with a 5% aqueous solution of hydrochloride acid and extracted with ether (3 x 100 mL). The combined organic layers were washed with water (100 mL), brine (100 mL), dried over anhydrous $MgSO_4$, filtered and dried under reduced pressure. The residue was purified by flash column chromatography (silica gel, 0-5% ether in hexanes) to yield 0.25 g (50 %) of compound 2 as colorless oil.

^{1}H NMR (400 MHz, $CDCl_3$) δ: ppm 5.43 – 5.28 (m, 8H), 3.58 (dd, *J* = 4.4 MHz, 1H), 2.78 (t, *J* = 6.6 MHz, 4H), 2.05 (q, *J* = 7.0, 8H), 1.51 – 1.22 (m, 45H), 0.89 (t, *J* = 6.8 MHz, 6H).

^{13}C NMR (101 MHz, CDCl3) δ: ppm 130.39, 130.34, 128.14, 128.12, 72.22, 37.69, 31.72, 29.90, 29.86, 29.80, 29.70, 29.55, 29.50, 27.42, 27.39, 25.86, 25.82, 22.77, 14.28.

Synthesis of [6Z,9Z,28Z,31Z)-heptatriaconta-6,9,28,31-tetraen-19-yl-4-(dimethylamino)butanoate] (Dlin-MC3-DMA).

A solution of compound 2 (0.2 g, 0.37 mmol) in dichloromethane (50 mL) was slowly added to a solution containing 4-dimethylaminobutyric acid hydrochloride (0.1 g, 0.63 mmol), *N*,*N*-diisopropylethylamine (0.1 mL, 12 mmol) and 4-dimethylaminopyridine (0.1 g, 0.66 mmol) in dichloromethane (10 mL). Then, a solution of 1-(3-dimethylaminopropyl)-3-ethylcarbodiimide hydrochloride (0.13 g, 0.66 mmol) in dichloromethane (10 mL) was added, and the resulting mixture was stirred overnight at room temperature. The reaction mixture was diluted with dichloromethane and washed with saturated $NaHCO_3$ (aq.) (100 mL), water (100 mL) and brine (100 mL). The organic phase was then dried over anhydrous $MgSO_4$, filtered and dried under reduced pressure. The residue was purified by flash column chromatography [silica gel, 0-5% methanol in dichloromethane (containing 1% NH_4OH)] to yield 0.13 g (65%) of Dlin-MC3-DMA as colorless oil.

^{1}H NMR (400 MHz, $CDCl_3$) δ: ppm 5.42 – 5.28 (m, 8H), 4.86 (qt, *J* = 6.2 MHz, 1H), 2.77 (t, *J* = 6.4 MHz, 4H), 2.32 (t, *J* = 7.4 MHz, 4H), 2.24 (s, 6H), 2.04 (q, *J* = 6.4 MHz, 8H), 1.80 (qt, *J* = 7.4 MHz, 2H), 1.50 (d, *J* = 5.6 MHz, 4H), 1.41 – 1.18 (m, 39H), 0.89 (t, *J* = 6.7 MHz, 6H).

^{13}C NMR (101 MHz, CDCl3) δ: ppm 173.57, 130.38, 130.33, 128.14, 128.11, 74.44, 59.13, 45.62, 34.33, 32.66, 31.71, 29.86, 29.75, 29.72, 29.68, 29.54, 29.49, 27.42, 27.38, 25.81, 25.53, 23.32, 22.77, 14.27.

HRMS (ESI): m/z calcd for $C_{43}H_{79}NO_2^+$ (M+H), 642.61; found, 642.61770.

4.1.3. Synthesis of ALC-0315

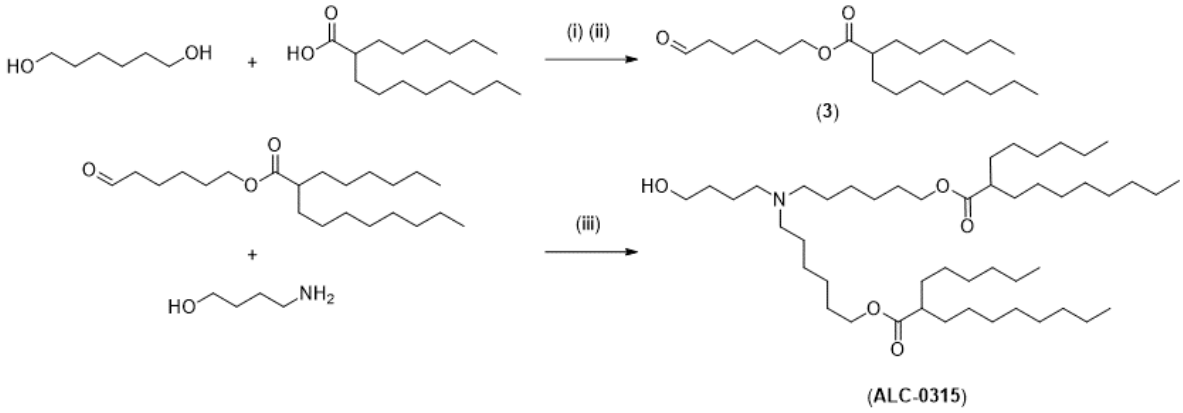

(i) EDCI, DMAP, DCM; (ii) PCC, DCM; (iii) STAB, CH_3COOH, DCM

Synthesis of 6-(2'-hexyldecanoyloxy)hexan-1-al (compound 3).

A solution containing 2-hexyldecanoic acid (19.8 g, 77.2 mmol), 1-(3-dimethylaminopropyl)-3-ethylcarbodiimide hydrochloride (18.2 g, 117.2 mmol) and 4-dimethylaminopyridine (11.3 g, 92.5 mmol) in dichloromethane (100 mL) was slowly added to a solution of hexan-1,6-diol (27.6 g, 233.6 mmol) in dichloromethane (400 mL). The reaction mixture was stirred for 72 h at room temperature. After that, the precipitated was removed by filtration, and the filtrate was diluted with hexane. The resulting mixture was stirred, and precipitates were allowed to settle out before it was filtered, washed with a diluted solution of hydrochloride acid, dried over anhydrous magnesium sulfate and filtered. The filtrate was evaporated to dryness under reduced pressure. The crude product was dissolved in dichloromethane (200 mL) and treated with pyridinum chlorochromate (15 g, 69.6 mmol) for 2 h at room temperature. Then, the reaction mixture was diluted with diethyl ether (500 mL), filtered through a silica gel bed, and the filtrate was evaporated to dryness under reduced pressure. The resulting oil was dissolved in hexane, and a suspension was formed, which was filtered through a silica gel plug, and the filtrate was dried under reduced pressure. The residue was passed down a silica gel column using hexane, followed by dichloromethane, as the eluent. After solvent removal, compound 3 (18.1 g, 60.3%) was obtained as a colorless oil.

^{1}H NMR (400 MHz, $CDCl_3$) δ: ppm 9.76 (t, *J* = 1.7 MHz, 1H), 4.09 – 4.02 (m, 2H), 2.43 (td, *J* = 7.5 MHz, 2H), 2.33 – 2.24 (m, 1H), 1.71 – 1.50 (m, 1H), 1.46 – 1.16 (m, 24H), 0.86 (t, *J* = 6.3 MHz, 6H).

^{13}C NMR (101 MHz, CDCl3) δ: ppm 202.41, 176.82, 64.08, 63.84, 45.99, 43.90, 32.70, 32.02, 31.87, 29.72, 29.62, 29.42, 29.38, 28.67, 27.64, 27.60, 25.75, 22.83, 22.75, 21.83, 14.27, 14.23.

Synthesis of [(4-Hydroxybutyl)azanediyl]di(hexane-6,1-diyl) bis(2-hexyldecanoate) (ALC-0315).

A solution containing compound 3 (5.0 g, 14.1 mmol), acetic acid (0.50 g, 8.3 mmol) and 4-amino-1-butan-1-ol (0.50 g, 5.6 mmol) in dichloromethane (20 mL) was treated with sodium triacetoxyborohydride (2.7 g, 12.7 mmol). The reaction mixture was stirred for 4 h at room temperature. The solution was washed with saturated $NaHCO_3$ (aq.) (100 mL), dried over anhydrous $MgSO_4$, filtered and dried under reduced pressure. The residue was purified by flash column chromatography (silica gel, 0-5% methanol in dichloromethane) to yield 0.9 g (18%) of ALC-0315 as slightly yellow oil.

^{1}H NMR (400 MHz, $CDCl_3$) δ: ppm 4.05 (t, *J* = 6.7 MHz, 4H), 3.64 – 3.55 (m, 2H), 2.57 (s, 6H), 2.35 – 2.25 (m, 2H), 1.76 – 1.17 (m, 70H), 0.87 (t, *J* = 6.1 MHz, 12H).

^{13}C NMR (101 MHz, CDCl3) δ: ppm 176.90, 64.08, 62.55, 53.51, 46.00, 32.69, 32.04, 31.88, 29.74, 29.44, 29.40, 28.81, 27.64, 27.60, 27.57, 27.29, 25.98, 22.85, 22.77, 14.30, 14.26.

HRMS (ESI): m/z calcd for $C_{48}H_{95}NO_5^+$ (M+H), 766.72; found, 766.72751.

4.1.4. Synthesis of SM-102

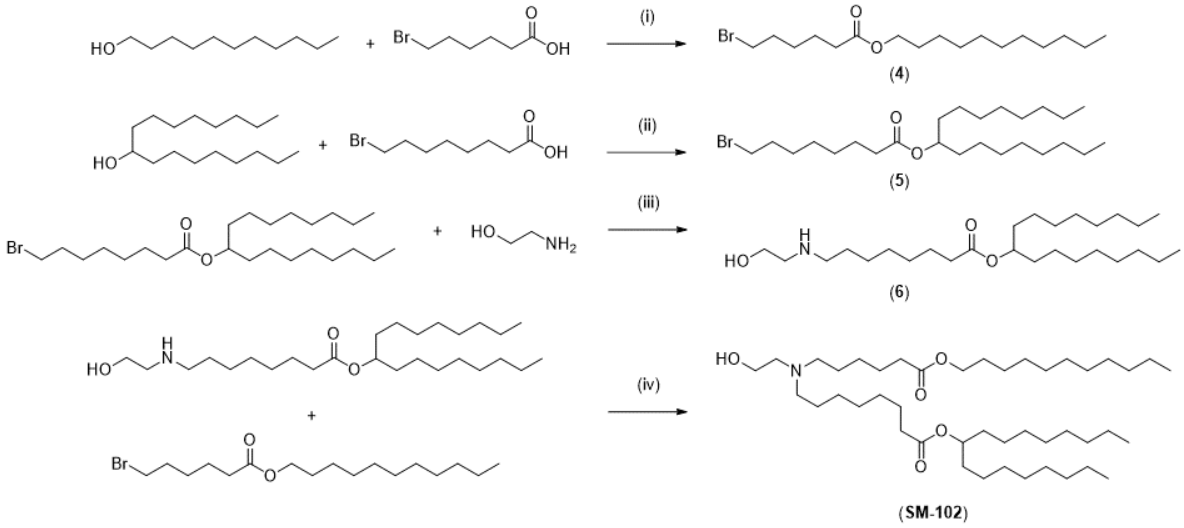

(i) (ii) EDCI, DMAP, DIPEA, DCM; (iii) EtOH; (iv) DIPEA, EtOH

Synthesis of undecyl 6-bromohexanoate (compound 4)

A solution containing 6-bromohexanoic acid (10 g, 51.3 mmol) and undecan-1-ol (17.7 g, 102.5 mmol) in dichloromethane (250 mL) was treated with 1-(3-dimethylaminopropyl)-3-ethylcarbodiimide hydrochloride (9.8 g, 51.3 mmol) and 4-dimethylaminopyridine (1.25 g, 10.3 mmol). The reaction mixture was stirred overnight at room temperature. The solution was diluted with dichloromethane (100 mL) and washed with saturated $NaHCO_3$ (aq.) (100 mL). The organic phase was washed with brine (100 mL), dried over anhydrous $MgSO_4$, filtered and dried under reduced pressure. The residue was purified by flash column chromatography (silica gel, 0-5% ethyl acetate in hexanes) to yield 14.3 g (80%) of compound 4 as colorless oil.

^{1}H NMR (400 MHz, $CDCl_3$) δ: ppm 3.50 (t, 2H), 3.37 (t, 2H), 2.29 (t, 2H), 1.91 – 1.76 (m, 2H), 1.74 – 1.16. (m, 22H), 0.91 – 0.81 (m, 3H).

Synthesis of heptadecan-9-yl 8-bromooctanoate (compound 5)

A solution containing 8-bromooctanoic acid (2.08 g, 9.2 mmol) and hepdecan-9-ol (3.0 g, 11.6 mmol) in dichloromethane (50 mL) was treated with 1-(3-dimethylaminopropyl)-3-ethylcarbodiimide hydrochloride (2.2 g, 11.6 mmol), *N*,*N*-diisopropylethylamine (6.6 mL, 37.4 mmol) and 4-dimethylaminopyridine (2.25 g, 20.6 mmol). The reaction mixture was stirred overnight at room temperature. The solution was diluted with dichloromethane and washed with saturated $NaHCO_3$ (aq.) (100 mL). The organic phase was washed with brine (100 mL), dried over anhydrous $MgSO_4$, filtered and dried under reduced pressure. The residue was purified by flash column chromatography (silica gel, 0-5% ethyl acetate in hexanes) to yield 2.08 g (48.7%) of compound 5 as slightly yellow oil.

^{1}H NMR (400 MHz, $CDCl_3$) δ: ppm 4.86 (qt, *J* = 6.3 MHz, 1H), 3.39 (t, *J* = 7.0 MHz, 2H), 2.27 (t, *J* = 7.2 MHz, 2H), 1.84 (qt, *J* = 7.8 MHz, 2H), 1.70 – 1.13 (m, 36H), 0.87 (t, *J* = 5.9 MHz, 6H).

^{13}C NMR (101 MHz, CDCl3) δ: ppm 173.72, 45.22, 34.80, 34.33, 34.03, 32.90, 32.04, 29.71, 29.69, 29.42, 29.13, 28.62, 28.18, 25.50, 25.20, 22.85, 14.28.

Synthesis of heptadecan-9-yl 8-((2-hydroxyethyl)amino)octanoate (compound 6)

A solution containing compound 5 (2.0 g, 4.3 mmol) and 2-aminoethan-1-ol (8 mL, 132.3 mmol) in ethanol (5 mL) was stirred and heated under reflux at 62 °C for 16 h. The solution was cooled to room temperature, concentrated under reduced pressure, and the residue was dissolved in ethyl acetate and washed with water (100 mL). The resulting organic layer was washed with brine (100 mL), dried over anhydrous $MgSO_4$, filtered and dried under reduced pressure. The residue was purified by flash column chromatography [silica gel, 0-10% methanol in dichloromethane (containing 1% NH_4OH)] to yield 1.5 g (75 %) of compound 6 as slightly yellow oil.

^{1}H NMR (400 MHz, $CDCl_3$) δ: ppm 4.85 (qt, *J* = 6.3 MHz, 1H), 3.77 (t, *J* = 5.2 MHz, 2H), 2.91 (t, *J* = 5.3 MHz, 2H), 2.76 (t, *J* = 7.1 MHz, 2H), 2.27 (t, *J* = 7.3 MHz, 2H), 1.74 – 1.41 (m, 8H), 1.40 – 1.13 (m, 30H), 0.87 (t, *J* = 6.9 MHz, 6H).

^{13}C NMR (101 MHz, CDCl3) δ: ppm 173.75, 74.37, 58.71, 50.80, 48.87, 34.77, 34.31, 32.04, 29.71, 29.68, 29.42, 29.17, 29.05, 27.43, 26.88, 25.50, 25.14, 22.85, 14.30.

Synthesis of heptadecan-9-yl 8-((2-hydroxyethyl)(6-oxo-6-(undecyloxy)hexyl)amino)octanoate (SM-102).

A solution containing compound 4 (0.76 g, 2.19 mmol), compound 6 (0.8 g, 1.81 mmol) and *N*,*N*-diisopropylethylamine (0.3 g, 2.3 mmol) in ethanol (5 mL) was stirred and heated under reflux at 62 °C for 16 h. The solution was cooled to room temperature, concentrated under reduced pressure, and the residue was dissolved in ethyl acetate and washed with saturated $NaHCO_3$ (aq.) (100 mL). The resulting organic layer was dried over anhydrous $MgSO_4$, filtered and dried under reduced pressure. The residue was purified by flash column chromatography [silica gel, 0-10% methanol in dichloromethane (containing 1% NH_4OH)] to yield 0.3 g (19 %) of SM-102 as slightly yellow oil.

^{1}H NMR (400 MHz, $CDCl_3$) δ: ppm 4.86 (qt, J = 6.1 MHz, 1H), 4.05 (t, J = 7.2 MHz, 2H), 3.53 (t, J = 5.5 MHz, 2H), 2.62 – 2.54 (m, 2H), 2.49 – 2.40 (m, 4H), 2.33 – 2.24 (m, 4H), 173 – 1.14 (m, 61H), 0.92 – 0.84 (m, 9H).

^{13}C NMR (101 MHz, CDCl3) δ: ppm 173.83, 74.30, 64.68, 58.45, 55.71, 53.98, 34.87, 34.47, 34.33, 32.05, 29.79, 29.72, 29.70, 29.52, 29.43, 29.41, 28.83, 27.47, 26.12, 25.51, 25.30, 25.07, 22.87, 14.31.

HRMS (ESI): m/z calcd for $C_{44}H_{87}NO_5^+$ (M+H), 710.666; found, 710.64487.

4.2. Supporting tables

Table S1. Physicochemical properties of the four DiD-labeled EGFP-mRNA-LNP formulations.

LNPs	Particle size (nm)	PDI	Zeta potential (mV)	EE (%)
DODAP	105.4 ± 1.0	0.190 ± 0.014	–15.67 ± 4.09	88.47 ± 3.16
Dlin-MC3-DMA	104.6 ± 1.2	0.144 ± 0.021	–12.36 ± 1.41	92.53 ± 1.92
ALC-0315	101.1 ± 1.4	0.122 ± 0.016	–13.03 ± 1.35	88.82 ± 4.52
SM-102	100.7 ± 1.2	0.159 ± 0.018	–9.13 ± 1.28	92.76 ± 1.58

Data were shown as mean ± SD of three independent experiments.

4.3. Supporting figures

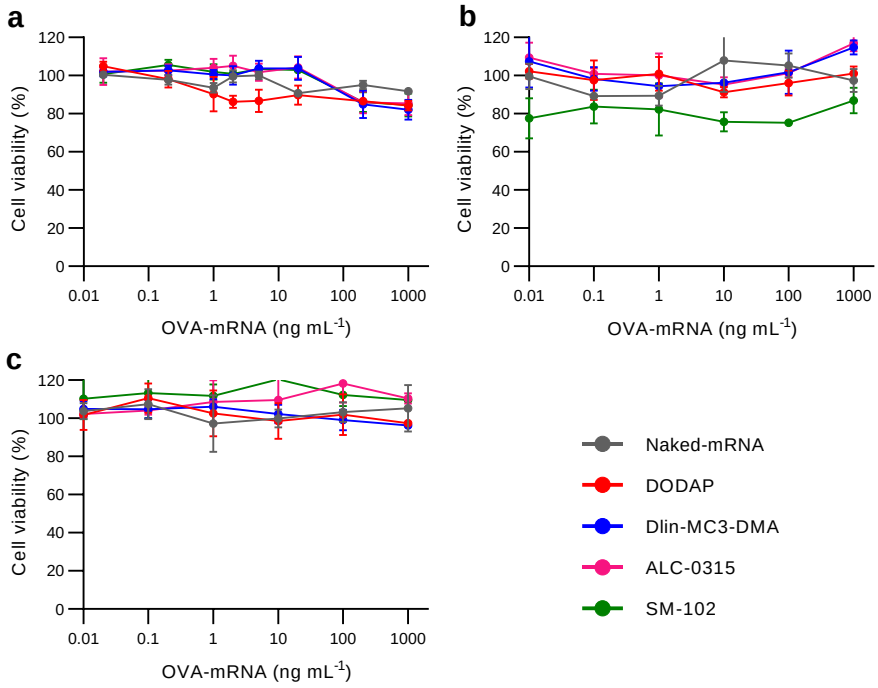

Figure S1. Cytotoxicity of OVA-mRNA-LNPs. Percentages of cell viability of naked OVA-mRNA, DODAP, Dlin-MC3-DMA, ALC-0315 and SM-102 on **a** BMDCs, **b** DC2.4 and **c** RAW264.7, as determined by cell viability assays. Data were shown as mean ± SD, n = 3.

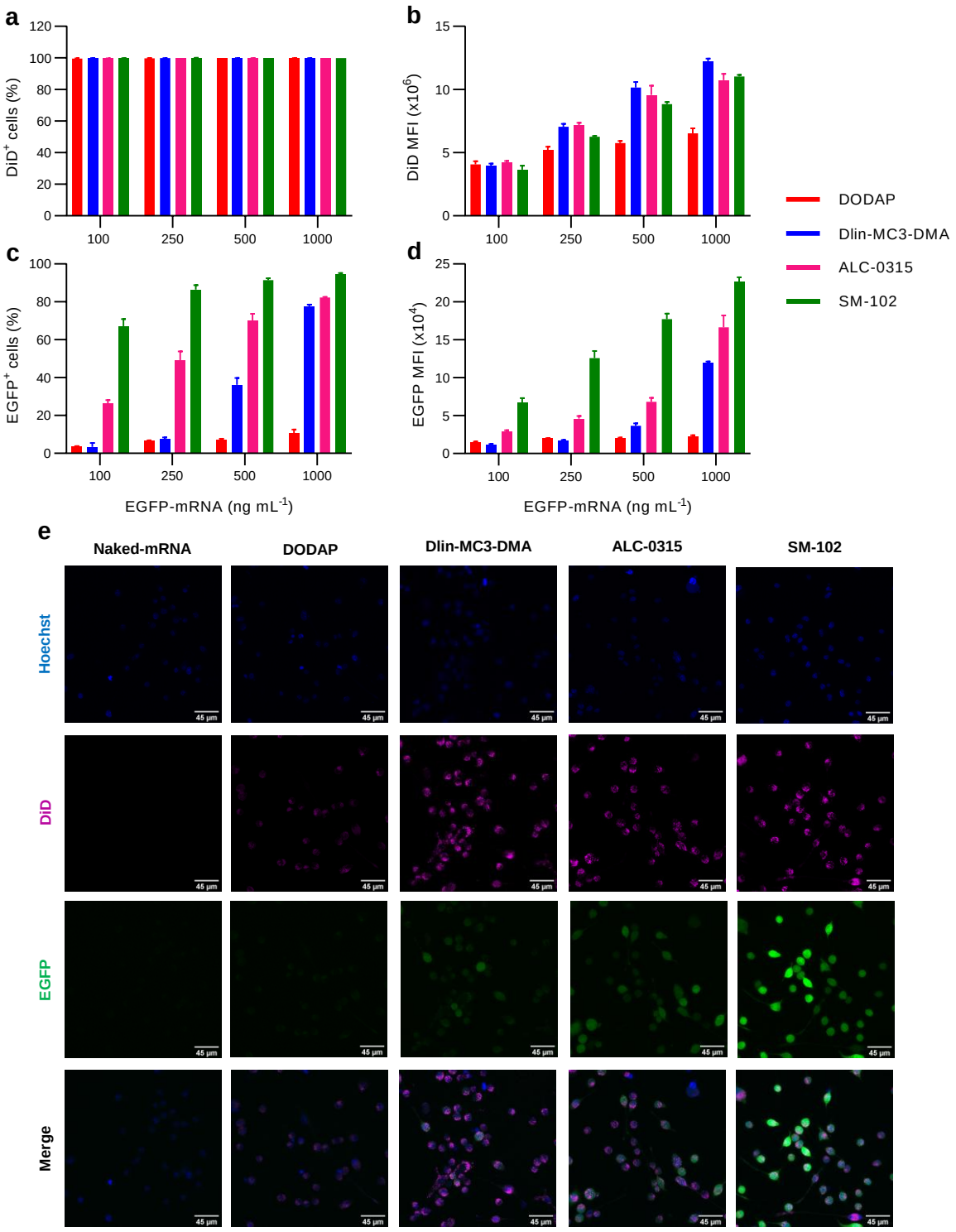

Figure S2. *In vitro* cellular uptake and transfection of the mRNA-LNPs in immortalized murine dendritic cells (DC2.4). **a-b** Cellular uptake and **c-d** EGFP expression after exposing DC2.4 with DiD-labeled EGFP-mRNA-LNPs at different EGFP-mRNA concentrations for 24 h, as determined by flow cytometry. **e** Confocal microscopy images of DC2.4 showing cellular uptake (magenta; DiD-labeled LNPs) and protein expression (green; EGFP) after 24 h of incubation. The Nucleus was stained with Hoechst (blue). Data were shown as mean ± SD, n = 3.

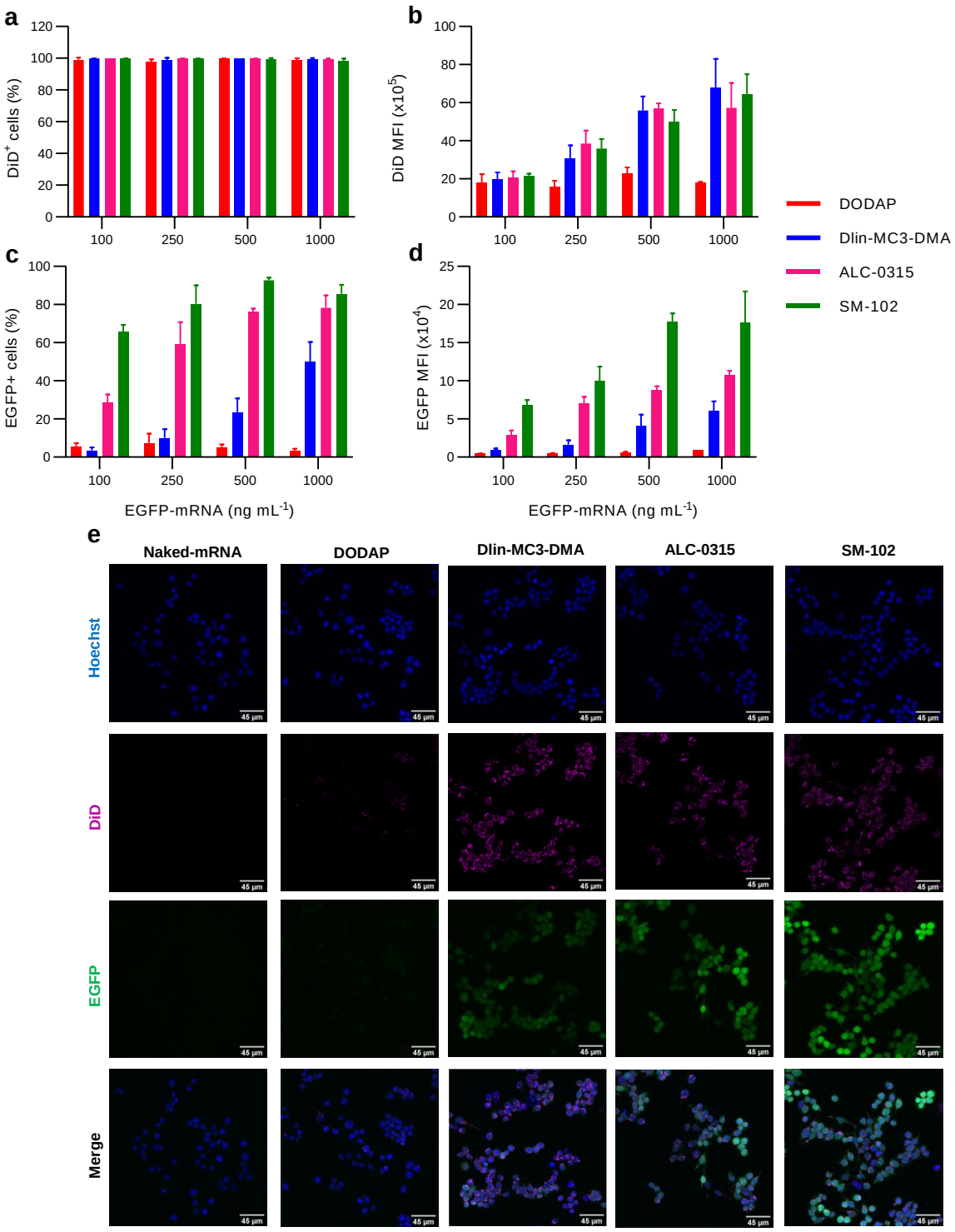

Figure S3. *In vitro* cellular uptake and transfection of the mRNA-LNPs in immortalized murine macrophage cells (RAW264.7). **a-b** Cellular uptake and **c-d** EGFP expression after exposing RAW264.7 with DiD-labeled EGFP-mRNA-LNPs at different EGFP-mRNA concentrations for 24 h, as determined by flow cytometry. **e** Confocal microscopy images of RAW264.7 showing cellular uptake (magenta; DiD-labeled LNPs) and protein expression (green; EGFP) after 24 h of incubation. The Nucleus was stained with Hoechst (blue). Data were shown as mean ± SD, n = 3; *p < 0.05, **p < 0.01 and ***p < 0.001.

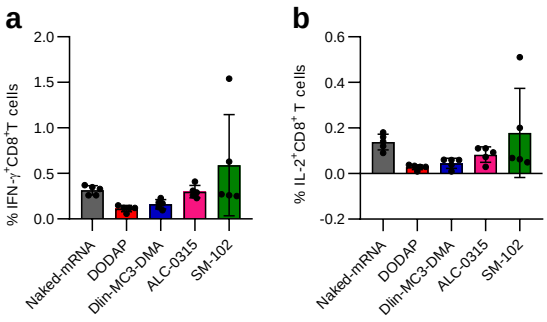

Figure S4. *In vivo* cellular immune response induced by the OVA-mRNA LNPs in mice. Percentages of **a** IFN-γ– and **b** IL-2–producing $CD8^+$ T cells after intravenous administration of naked OVA-mRNA, DODAP, Dlin-MC3-DMA, ALC-0315 or SM-102 in mice (OVA-mRNA dose: 0.25 mg kg^{-1}), as determined by flow cytometry. Data are shown as mean ± SD, n = 5; *p < 0.05, **p < 0.01 and ***p < 0.001.

4.4. Spectra

^{1}H NMR spectrum of Dlin-MC3-DMA

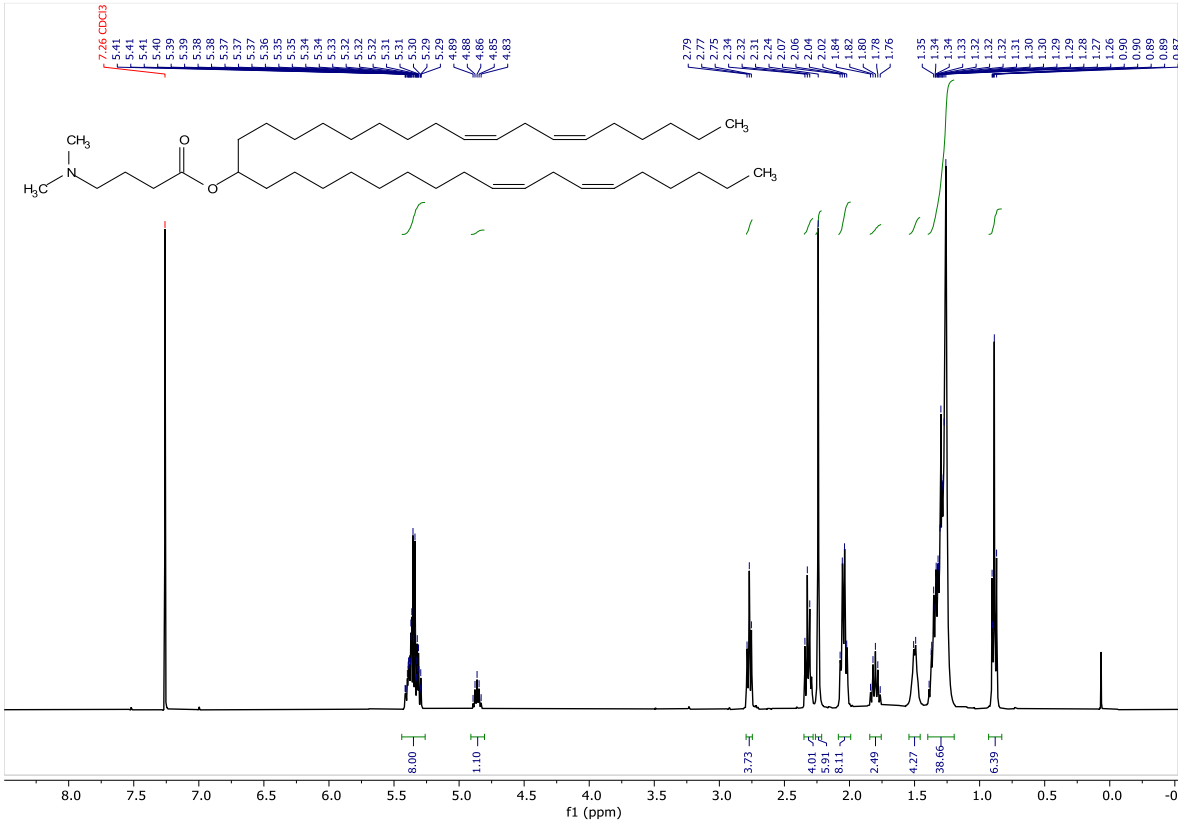

^{13}C NMR spectrum of Dlin-MC3-DMA

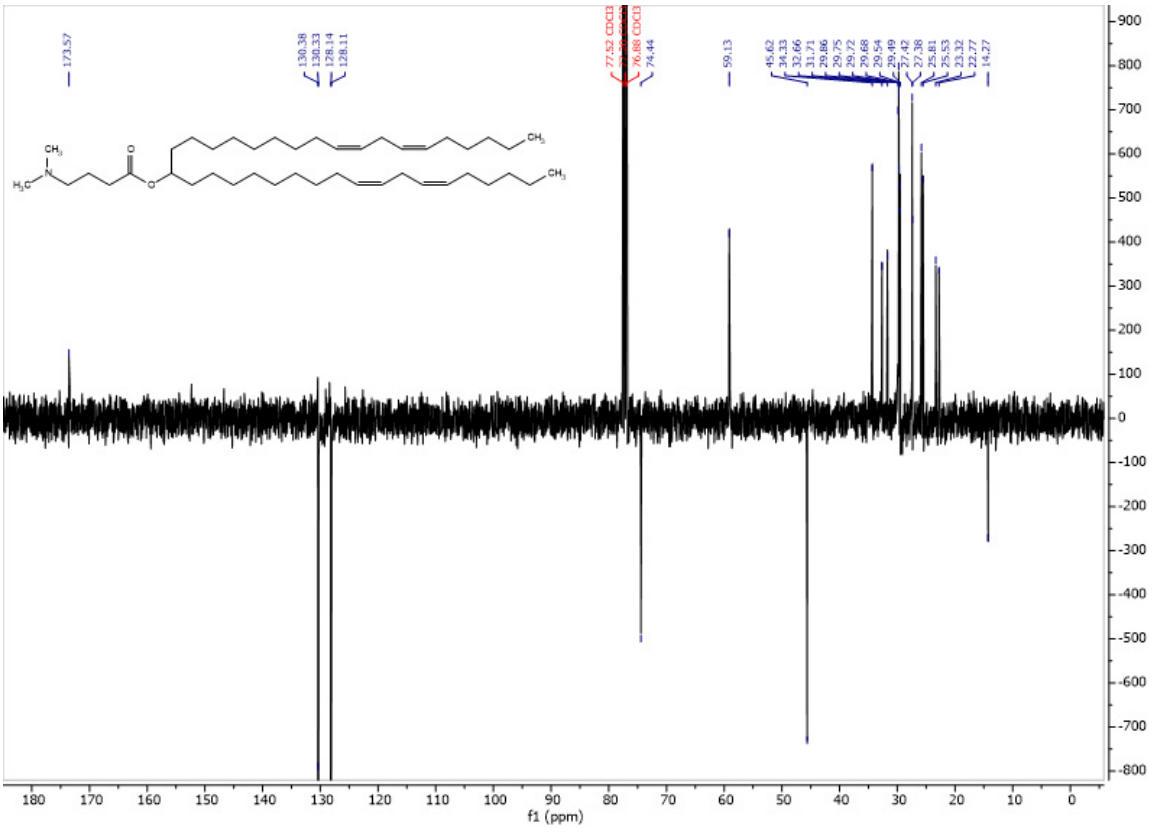

HRMS spectrum of Dlin-MC3-DMA

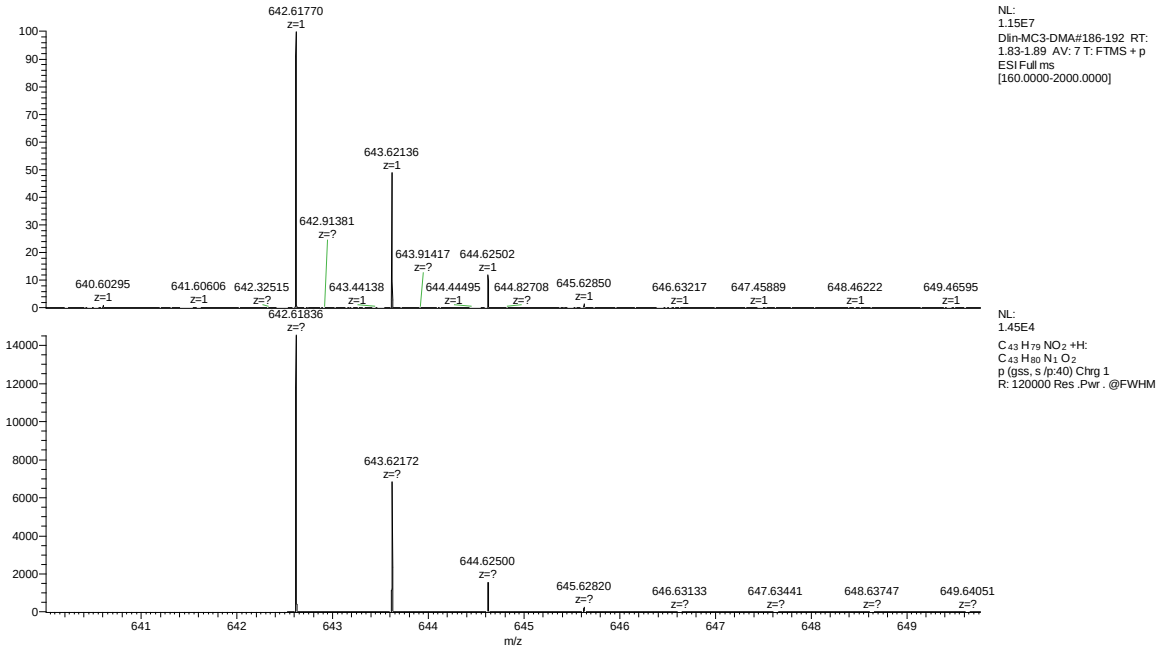

^{1}H NMR spectrum of ALC-0315

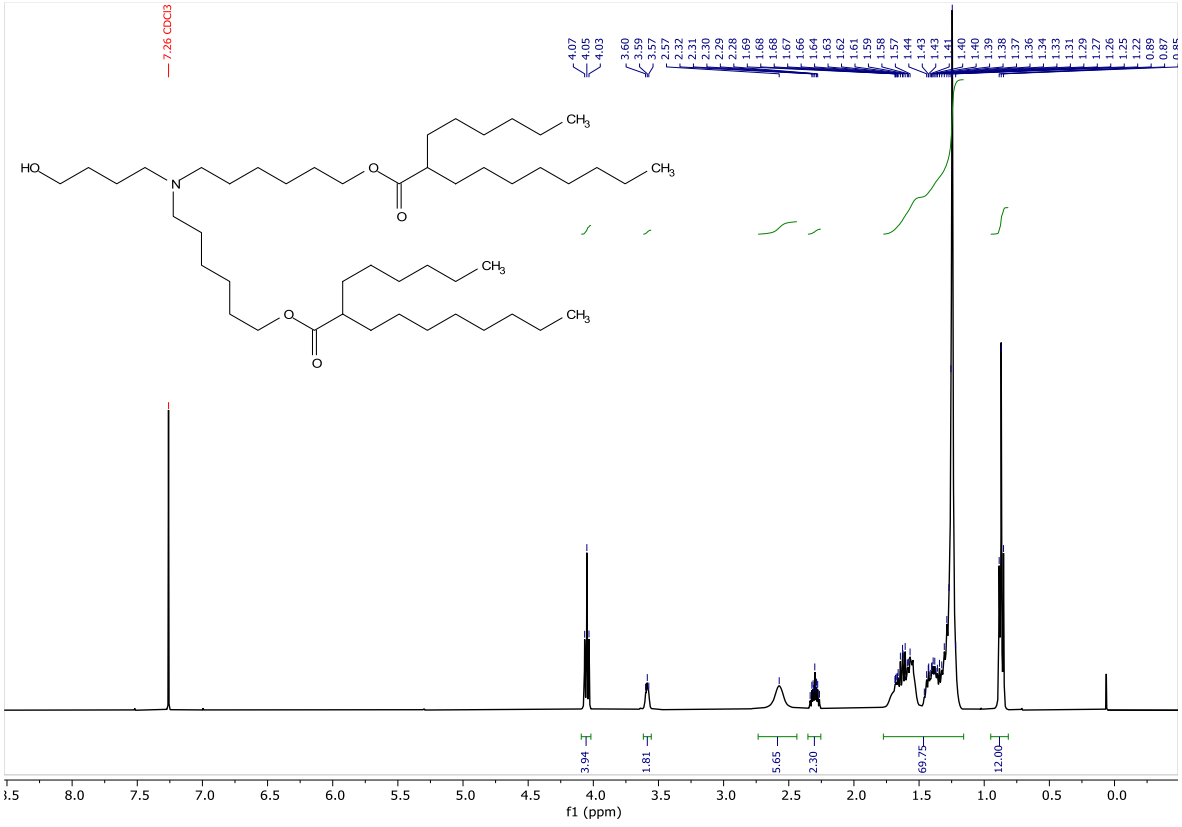

^{13}C NMR spectrum of ALC-0315

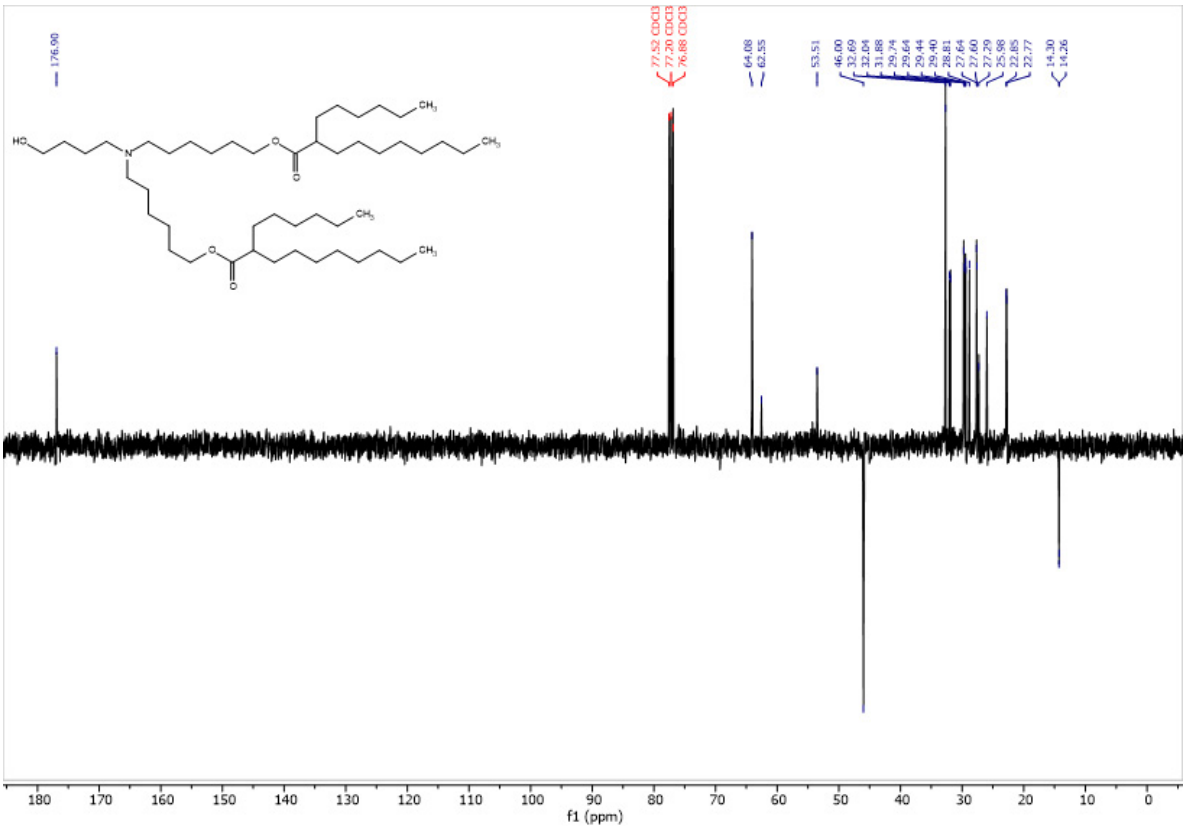

HRMS spectrum of ALC-0315

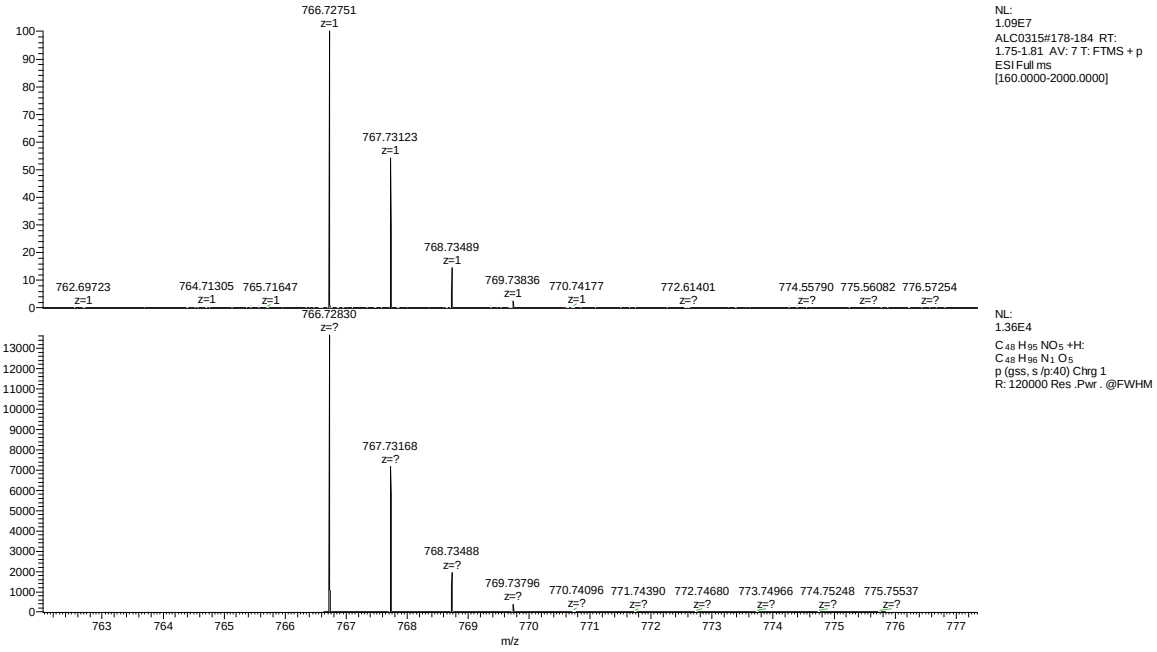

^{1}H NMR spectrum of SM-102

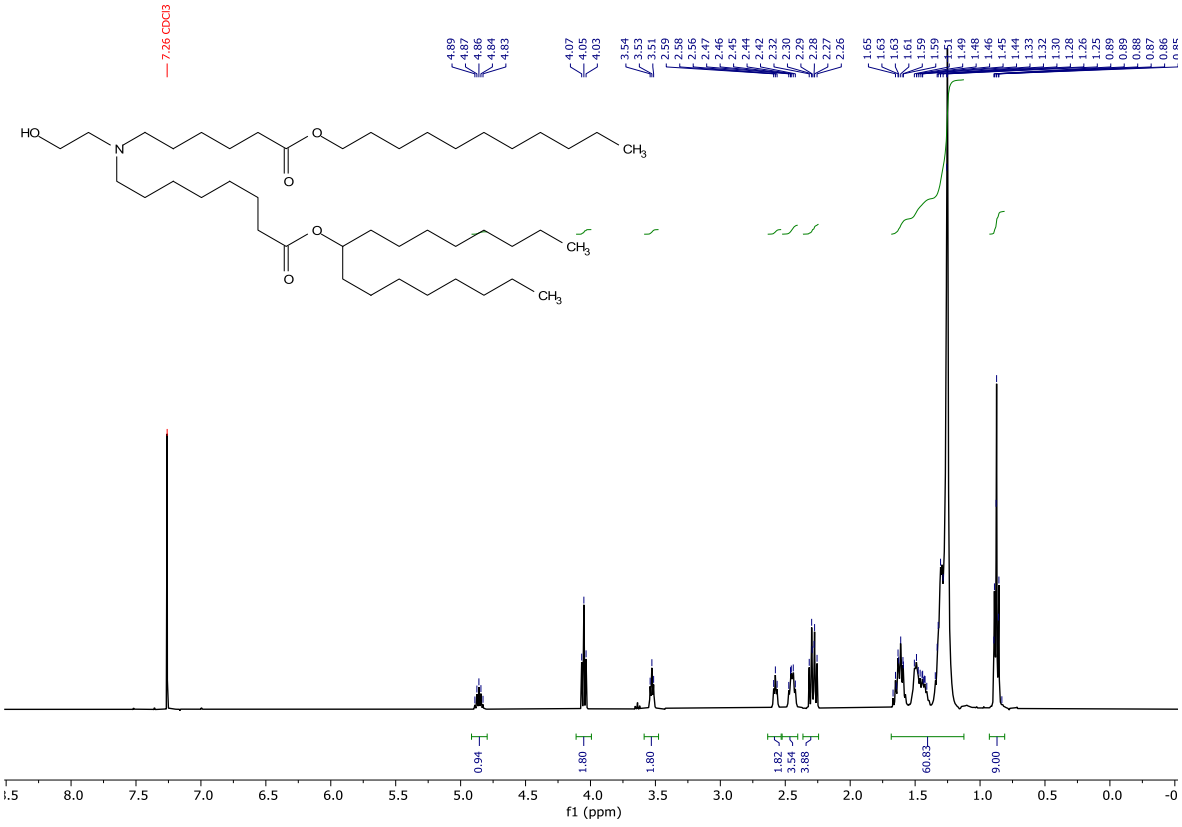

^{13}C NMR spectrum of ALC-0315

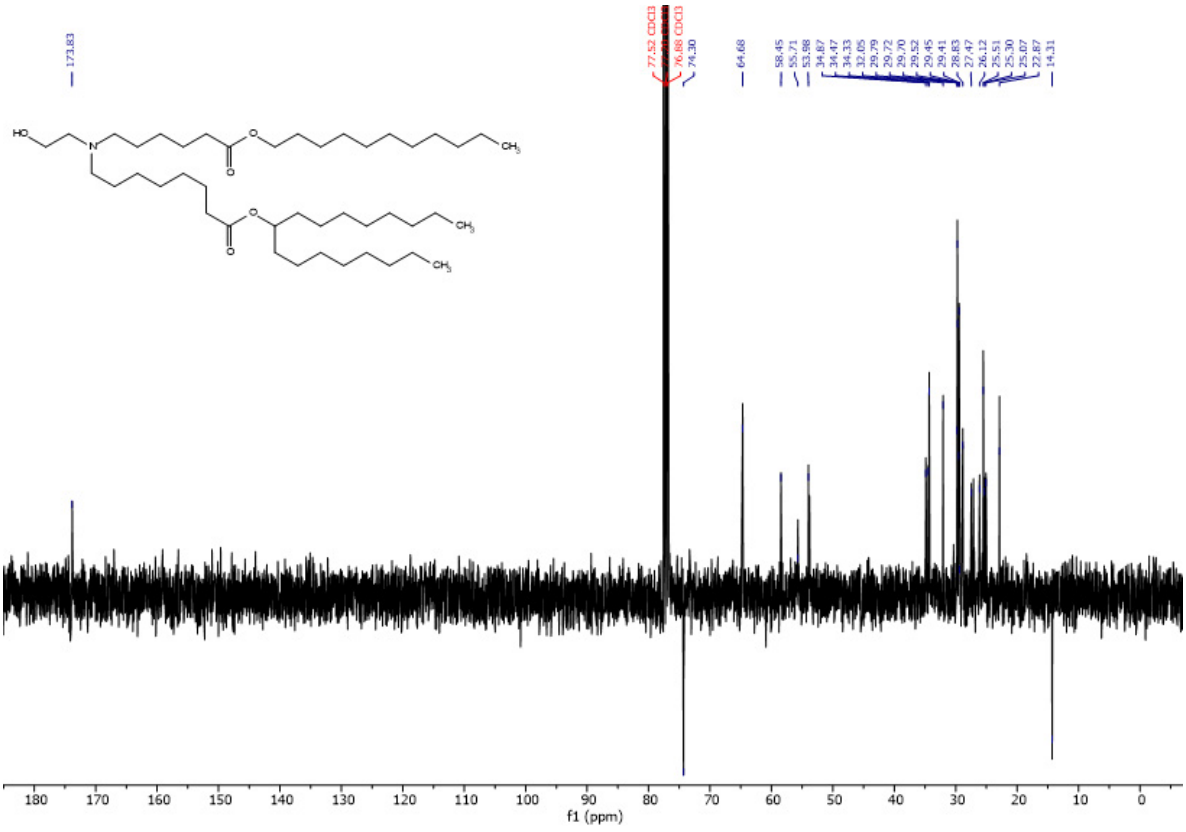

HRMS spectrum of SM-102

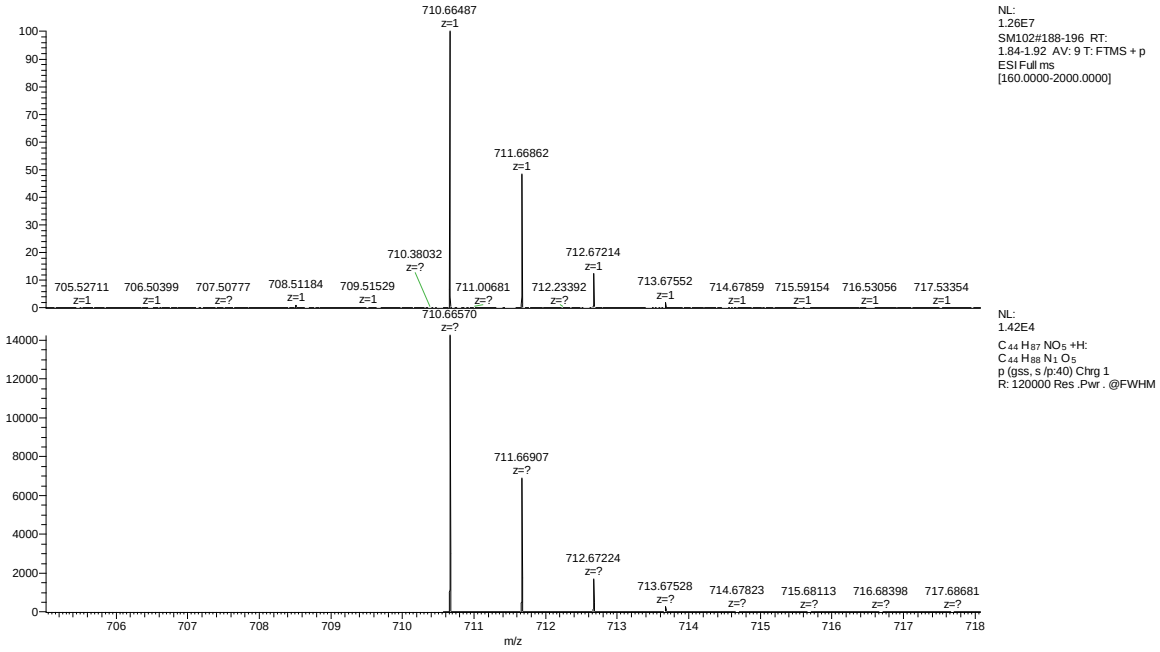

5. References

[1] U. Sahin, K. Karikó, Ö. Türeci, mRNA-based therapeutics — developing a new class of drugs, Nat Rev Drug Discov 13 (2014) 759–780. https://doi.org/10.1038/nrd4278.

[2] N. Pardi, M.J. Hogan, F.W. Porter, D. Weissman, mRNA vaccines — a new era in vaccinology, Nat Rev Drug Discov 17 (2018) 261–279. https://doi.org/10.1038/nrd.2017.243.

[3] A.J. Barbier, A.Y. Jiang, P. Zhang, R. Wooster, D.G. Anderson, The clinical progress of mRNA vaccines and immunotherapies, Nat Biotechnol 40 (2022) 840–854. https://doi.org/10.1038/s41587-022-01294-2.

[4] A.S. Lauring, M.W. Tenforde, J.D. Chappell, M. Gaglani, A.A. Ginde, T. McNeal, S. Ghamande, D.J. Douin, H.K. Talbot, J.D. Casey, N.M. Mohr, A. Zepeski, N.I. Shapiro, K.W. Gibbs, D.C. Files, D.N. Hager, A. Shehu, M.E. Prekker, H.L. Erickson, M.C. Exline, M.N. Gong, A. Mohamed, N.J. Johnson, V. Srinivasan, J.S. Steingrub, I.D. Peltan, S.M. Brown, E.T. Martin, A.S. Monto, A. Khan, C.L. Hough, L.W. Busse, C.C. ten Lohuis, A. Duggal, J.G. Wilson, A.J. Gordon, N. Qadir, S.Y. Chang, C. Mallow, C. Rivas, H.M. Babcock, J.H. Kwon, N. Halasa, C.G. Grijalva, T.W. Rice, W.B. Stubblefield, A. Baughman, K.N. Womack, J.P. Rhoads, C.J. Lindsell, K.W. Hart, Y. Zhu, K. Adams, S.J. Schrag, S.M. Olson, M. Kobayashi, J.R. Verani, M.M. Patel, W.H. Self, Clinical severity of, and effectiveness of mRNA vaccines against, covid-19 from omicron, delta, and alpha SARS-CoV-2 variants in the United States: prospective observational study, BMJ (2022) e069761. https://doi.org/10.1136/bmj-2021-069761.

[5] M.J. Hogan, N. Pardi, mRNA vaccines in the COVID-19 pandemic and beyond, Annu Rev Med 73 (2022) 17–39. https://doi.org/10.1146/annurev-med-042420-112725.

[6] P.S. Kowalski, A. Rudra, L. Miao, D.G. Anderson, Delivering the messenger: Advances in technologies for therapeutic mRNA delivery, Molecular Therapy 27 (2019) 710–728. https://doi.org/10.1016/j.ymthe.2019.02.012.

[7] L. Schoenmaker, D. Witzigmann, J.A. Kulkarni, R. Verbeke, G. Kersten, W. Jiskoot, D.J.A. Crommelin, mRNA-lipid nanoparticle COVID-19 vaccines: Structure and stability, Int J Pharm 601 (2021) 120586. https://doi.org/10.1016/j.ijpharm.2021.120586.

[8] X. Hou, T. Zaks, R. Langer, Y. Dong, Lipid nanoparticles for mRNA delivery, Nat Rev Mater 6 (2021) 1078–1094. https://doi.org/10.1038/s41578-021-00358-0.

[9] M.J. Mitchell, M.M. Billingsley, R.M. Haley, M.E. Wechsler, N.A. Peppas, R. Langer, Engineering precision nanoparticles for drug delivery, Nat Rev Drug Discov 20 (2021) 101–124. https://doi.org/10.1038/s41573-020-0090-8.

[10] D. Adams, A. Gonzalez-Duarte, W.D. O'Riordan, C.-C. Yang, M. Ueda, A. V. Kristen, I. Tournev, H.H. Schmidt, T. Coelho, J.L. Berk, K.-P. Lin, G. Vita, S. Attarian, V. Planté-Bordeneuve, M.M. Mezei, J.M. Campistol, J. Buades, T.H. Brannagan, B.J. Kim, J. Oh, Y. Parman, Y. Sekijima, P.N. Hawkins, S.D. Solomon, M. Polydefkis, P.J. Dyck, P.J. Gandhi, S. Goyal, J. Chen, A.L. Strahs, S. V. Nochur, M.T. Sweetser, P.P. Garg, A.K. Vaishnaw, J.A. Gollob, O.B. Suhr, Patisiran, an RNAi therapeutic, for hereditary transthyretin amyloidosis, New England Journal of Medicine 379 (2018) 11–21. https://doi.org/10.1056/NEJMoa1716153.

[11] F.P. Polack, S.J. Thomas, N. Kitchin, J. Absalon, A. Gurtman, S. Lockhart, J.L. Perez, G. Pérez Marc, E.D. Moreira, C. Zerbini, R. Bailey, K.A. Swanson, S. Roychoudhury,

K. Koury, P. Li, W. V. Kalina, D. Cooper, R.W. Frenck, L.L. Hammitt, Ö. Türeci, H. Nell, A. Schaefer, S. Ünal, D.B. Tresnan, S. Mather, P.R. Dormitzer, U. Şahin, K.U. Jansen, W.C. Gruber, Safety and efficacy of the BNT162b2 mRNA Covid-19 vaccine, New England Journal of Medicine 383 (2020) 2603–2615. https://doi.org/10.1056/NEJMoa2034577.

[12] L.R. Baden, H.M. El Sahly, B. Essink, K. Kotloff, S. Frey, R. Novak, D. Diemert, S.A. Spector, N. Rouphael, C.B. Creech, J. McGettigan, S. Khetan, N. Segall, J. Solis, A. Brosz, C. Fierro, H. Schwartz, K. Neuzil, L. Corey, P. Gilbert, H. Janes, D. Follmann, M. Marovich, J. Mascola, L. Polakowski, J. Ledgerwood, B.S. Graham, H. Bennett, R. Pajon, C. Knightly, B. Leav, W. Deng, H. Zhou, S. Han, M. Ivarsson, J. Miller, T. Zaks, Efficacy and safety of the mRNA-1273 SARS-CoV-2 vaccine, New England Journal of Medicine 384 (2021) 403–416. https://doi.org/10.1056/NEJMoa2035389.

[13] C. Hald Albertsen, J.A. Kulkarni, D. Witzigmann, M. Lind, K. Petersson, J.B. Simonsen, The role of lipid components in lipid nanoparticles for vaccines and gene therapy, Adv Drug Deliv Rev 188 (2022) 114416. https://doi.org/10.1016/j.addr.2022.114416.

[14] P. Patel, N.M. Ibrahim, K. Cheng, The importance of apparent pKa in the development of nanoparticles encapsulating siRNA and mRNA, Trends Pharmacol Sci 42 (2021) 448–460. https://doi.org/10.1016/j.tips.2021.03.002.

[15] M. Schlich, R. Palomba, G. Costabile, S. Mizrahy, M. Pannuzzo, D. Peer, P. Decuzzi, Cytosolic delivery of nucleic acids: The case of ionizable lipid nanoparticles, Bioeng Transl Med 6 (2021). https://doi.org/10.1002/btm2.10213.

[16] P. Karmacharya, B.R. Patil, J.O. Kim, Recent advancements in lipid–mRNA nanoparticles as a treatment option for cancer immunotherapy, J Pharm Investig 52 (2022) 415–426. https://doi.org/10.1007/s40005-022-00569-9.

[17] X. Han, H. Zhang, K. Butowska, K.L. Swingle, M.-G. Alameh, D. Weissman, M.J. Mitchell, An ionizable lipid toolbox for RNA delivery, Nat Commun 12 (2021) 7233. https://doi.org/10.1038/s41467-021-27493-0.

[18] S.M. Gruner, P.R. Cullis, M.J. Hope, C.P.S. Tilcock, Lipid polymorphism:The molecular basis of nonbilayer phases, Annu Rev Biophys Biophys Chem 14 (1985) 211–238. https://doi.org/10.1146/annurev.bb.14.060185.001235.

[19] M.D. Buschmann, M.J. Carrasco, S. Alishetty, M. Paige, M.G. Alameh, D. Weissman, Nanomaterial delivery systems for mRNA vaccines, Vaccines (Basel) 9 (2021) 65. https://doi.org/10.3390/vaccines9010065.

[20] M.J. Carrasco, S. Alishetty, M.-G. Alameh, H. Said, L. Wright, M. Paige, O. Soliman, D. Weissman, T.E. Cleveland, A. Grishaev, M.D. Buschmann, Ionization and structural properties of mRNA lipid nanoparticles influence expression in intramuscular and intravascular administration, Commun Biol 4 (2021) 956. https://doi.org/10.1038/s42003-021-02441-2.

[21] S. Berger, M. Berger, C. Bantz, M. Maskos, E. Wagner, Performance of nanoparticles for biomedical applications: The in vitro/in vivo discrepancy, Biophys Rev 3 (2022). https://doi.org/10.1063/5.0073494.

[22] K. Paunovska, C.D. Sago, C.M. Monaco, W.H. Hudson, M.G. Castro, T.G. Rudoltz, S. Kalathoor, D.A. Vanover, P.J. Santangelo, R. Ahmed, A. V. Bryksin, J.E. Dahlman, A direct comparison of in vitro and in vivo nucleic acid delivery mediated by hundreds of

nanoparticles reveals a weak correlation, Nano Lett 18 (2018) 2148–2157. https://doi.org/10.1021/acs.nanolett.8b00432.

[23] F. Ferraresso, A.W. Strilchuk, L.J. Juang, L.G. Poole, J.P. Luyendyk, C.J. Kastrup, Comparison of DLin-MC3-DMA and ALC-0315 for siRNA delivery to hepatocytes and hepatic stellate cells, Mol Pharm 19 (2022) 2175–2182. https://doi.org/10.1021/acs.molpharmaceut.2c00033.

[24] K.J. Hassett, K.E. Benenato, E. Jacquinet, A. Lee, A. Woods, O. Yuzhakov, S. Himansu, J. Deterling, B.M. Geilich, T. Ketova, C. Mihai, A. Lynn, I. McFadyen, M.J. Moore, J.J. Senn, M.G. Stanton, Ö. Almarsson, G. Ciaramella, L.A. Brito, Optimization of lipid nanoparticles for intramuscular administration of mRNA vaccines, Mol Ther Nucleic Acids 15 (2019) 1–11. https://doi.org/10.1016/j.omtn.2019.01.013.

[25] A.L. Bailey, P.R. Cullis, Membrane fusion with cationic liposomes: Effects of target membrane lipid composition, Biochemistry 36 (1997) 1628–1634. https://doi.org/10.1021/bi961173x.

[26] M. Yanez Arteta, T. Kjellman, S. Bartesaghi, S. Wallin, X. Wu, A.J. Kvist, A. Dabkowska, N. Székely, A. Radulescu, J. Bergenholtz, L. Lindfors, Successful reprogramming of cellular protein production through mRNA delivered by functionalized lipid nanoparticles, Proceedings of the National Academy of Sciences 115 (2018) E3351–E3360. https://doi.org/10.1073/pnas.1720542115.

[27] P. Zhao, X. Hou, J. Yan, S. Du, Y. Xue, W. Li, G. Xiang, Y. Dong, Long-term storage of lipid-like nanoparticles for mRNA delivery, Bioact Mater 5 (2020) 358–363. https://doi.org/10.1016/j.bioactmat.2020.03.001.

[28] B. Kim, R.R. Hosn, T. Remba, D. Yun, N. Li, W. Abraham, M.B. Melo, M. Cortes, B. Li, Y. Zhang, Y. Dong, D.J. Irvine, Optimization of storage conditions for lipid nanoparticle-formulated self-replicating RNA vaccines, Journal of Controlled Release 353 (2023) 241–253. https://doi.org/10.1016/j.jconrel.2022.11.022.

[29] J. Viger-Gravel, A. Schantz, A.C. Pinon, A.J. Rossini, S. Schantz, L. Emsley, Structure of lipid nanoparticles containing siRNA or mRNA by dynamic nuclear polarization-enhanced NMR spectroscopy, J Phys Chem B 122 (2018) 2073–2081. https://doi.org/10.1021/acs.jpcb.7b10795.

[30] J.H. Park, N. Oh, Endocytosis and exocytosis of nanoparticles in mammalian cells, Int J Nanomedicine 9 (2014) 51–63. https://doi.org/10.2147/IJN.S26592.

[31] S. Salatin, S. Maleki Dizaj, A. Yari Khosroushahi, Effect of the surface modification, size, and shape on cellular uptake of nanoparticles, Cell Biol Int 39 (2015) 881–890. https://doi.org/10.1002/cbin.10459.

[32] A. Albanese, P.S. Tang, W.C.W. Chan, The effect of nanoparticle size, shape, and surface chemistry on biological systems, Annu Rev Biomed Eng 14 (2012) 1–16. https://doi.org/10.1146/annurev-bioeng-071811-150124.

[33] P. Paramasivam, C. Franke, M. Stöter, A. Höijer, S. Bartesaghi, A. Sabirsh, L. Lindfors, M.Y. Arteta, A. Dahlén, A. Bak, S. Andersson, Y. Kalaidzidis, M. Bickle, M. Zerial, Endosomal escape of delivered mRNA from endosomal recycling tubules visualized at the nanoscale, Journal of Cell Biology 221 (2022) e202110137. https://doi.org/10.1083/jcb.202110137.

[34] Y.-B. Hu, E.B. Dammer, R.-J. Ren, G. Wang, The endosomal-lysosomal system: from acidification and cargo sorting to neurodegeneration, Transl Neurodegener 4 (2015) 18. https://doi.org/10.1186/s40035-015-0041-1.

[35] M.J. Hope, B. Mui, P. Lin, J. Ching, C. Barbosa, T. Madden, S.M. Ansell, X. Du, Lipid nanoparticle formulations, WO2018081480A1, 2017.

[36] J. Gilleron, W. Querbes, A. Zeigerer, A. Borodovsky, G. Marsico, U. Schubert, K. Manygoats, S. Seifert, C. Andree, M. Stöter, H. Epstein-Barash, L. Zhang, V. Koteliansky, K. Fitzgerald, E. Fava, M. Bickle, Y. Kalaidzidis, A. Akinc, M. Maier, M. Zerial, Image-based analysis of lipid nanoparticle–mediated siRNA delivery, intracellular trafficking and endosomal escape, Nat Biotechnol 31 (2013) 638–646. https://doi.org/10.1038/nbt.2612.

[37] Y. Eygeris, S. Patel, A. Jozic, G. Sahay, Deconvoluting lipid nanoparticle structure for messenger RNA delivery, Nano Lett 20 (2020) 4543–4549. https://doi.org/10.1021/acs.nanolett.0c01386.

[38] P. Jin, T.H. Han, J. Ren, S. Saunders, E. Wang, F.M. Marincola, D.F. Stroncek, Molecular signatures of maturing dendritic cells: implications for testing the quality of dendritic cell therapies, J Transl Med 8 (2010) 4. https://doi.org/10.1186/1479-5876-8-4.

[39] K.L. Griffiths, J.K. Tan, H.C. O'Neill, Characterization of the effect of LPS scp on dendritic cell subset discrimination in spleen, J Cell Mol Med 18 (2014) 1908–1912. https://doi.org/10.1111/jcmm.12332.

[40] K.C. Howland, L.J. Ausubel, C.A. London, A.K. Abbas, The roles of CD28 and CD40 ligand in T cell activation and tolerance, The Journal of Immunology 164 (2000) 4465–4470. https://doi.org/10.4049/jimmunol.164.9.4465.

[41] A. Isser, A.B. Silver, H.C. Pruitt, M. Mass, E.H. Elias, G. Aihara, S.-S. Kang, N. Bachmann, Y.-Y. Chen, E.K. Leonard, J.G. Bieler, W. Chaisawangwong, J. Choy, S.R. Shannon, S. Gerecht, J.S. Weber, J.B. Spangler, J.P. Schneck, Nanoparticle-based modulation of CD4+ T cell effector and helper functions enhances adoptive immunotherapy, Nat Commun 13 (2022) 6086. https://doi.org/10.1038/s41467-022-33597-y.

[42] M. Barberis, T. Helikar, P. Verbruggen, Simulation of stimulation: Cytokine dosage and cell cycle crosstalk driving timing-dependent T cell differentiation, Front Physiol 9 (2018) 879. https://doi.org/10.3389/fphys.2018.00879.

[43] S.-D. Li, L. Huang, Pharmacokinetics and biodistribution of nanoparticles, Mol Pharm 5 (2008) 496–504. https://doi.org/10.1021/mp800049w.

[44] R. Pattipeiluhu, G. Arias-Alpizar, G. Basha, K.Y.T. Chan, J. Bussmann, T.H. Sharp, M. Moradi, N. Sommerdijk, E.N. Harris, P.R. Cullis, A. Kros, D. Witzigmann, F. Campbell, Anionic lipid nanoparticles preferentially deliver mRNA to the hepatic reticuloendothelial system, Advanced Materials 34 (2022) e2201095. https://doi.org/10.1002/adma.202201095.

[45] S. Sieber, P. Grossen, J. Bussmann, F. Campbell, A. Kros, D. Witzigmann, J. Huwyler, Zebrafish as a preclinical in vivo screening model for nanomedicines, Adv Drug Deliv Rev 151–152 (2019) 152–168. https://doi.org/10.1016/j.addr.2019.01.001.

[46] Y. Fang, J. Xue, S. Gao, A. Lu, D. Yang, H. Jiang, Y. He, K. Shi, Cleavable PEGylation: A strategy for overcoming the "PEG dilemma" in efficient drug delivery, Drug Deliv 24 (2017) 22–32. https://doi.org/10.1080/10717544.2017.1388451.

[47] X. Zhu, W. Tao, D. Liu, J. Wu, Z. Guo, X. Ji, Z. Bharwani, L. Zhao, X. Zhao, O.C. Farokhzad, J. Shi, Surface de-PEGylation controls nanoparticle-mediated siRNA delivery in vitro and in vivo, Theranostics 7 (2017) 1990–2002. https://doi.org/10.7150/thno.18136.

[48] B.L. Mui, Y.K. Tam, M. Jayaraman, S.M. Ansell, X. Du, Y.Y.C. Tam, P.J. Lin, S. Chen, J.K. Narayanannair, K.G. Rajeev, M. Manoharan, A. Akinc, M.A. Maier, P. Cullis, T.D. Madden, M.J. Hope, Influence of polyethylene glycol lipid desorption rates on pharmacokinetics and pharmacodynamics of siRNA lipid nanoparticles, Mol Ther Nucleic Acids 2 (2013) e139. https://doi.org/10.1038/mtna.2013.66.

[49] T. Suzuki, Y. Suzuki, T. Hihara, K. Kubara, K. Kondo, K. Hyodo, K. Yamazaki, T. Ishida, H. Ishihara, PEG shedding-rate-dependent blood clearance of PEGylated lipid nanoparticles in mice: Faster PEG shedding attenuates anti-PEG IgM production, Int J Pharm 588 (2020) 119792. https://doi.org/10.1016/j.ijpharm.2020.119792.

[50] V. Francia, R.M. Schiffelers, P.R. Cullis, D. Witzigmann, The biomolecular corona of lipid nanoparticles for gene therapy, Bioconjug Chem 31 (2020) 2046–2059. https://doi.org/10.1021/acs.bioconjchem.0c00366.

[51] Y. Zeng, O. Escalona-Rayo, R. Knol, A. Kros, B. Slütter, Lipid nanoparticle-based mRNA candidates elicit potent T cell responses, Biomater Sci 11 (2023) 964–974. https://doi.org/10.1039/D2BM01581A.

[52] G. Arias-Alpizar, L. Kong, R.C. Vlieg, A. Rabe, P. Papadopoulou, M.S. Meijer, S. Bonnet, S. Vogel, J. van Noort, A. Kros, F. Campbell, Light-triggered switching of liposome surface charge directs delivery of membrane impermeable payloads in vivo, Nat Commun 11 (2020) 3638. https://doi.org/10.1038/s41467-020-17360-9.

[53] F. Campbell, F.L. Bos, S. Sieber, G. Arias-Alpizar, B.E. Koch, J. Huwyler, A. Kros, J. Bussmann, Directing nanoparticle biodistribution through evasion and exploitation of Stab2-dependent nanoparticle uptake, ACS Nano 12 (2018) 2138–2150. https://doi.org/10.1021/acsnano.7b06995.

[54] M. Qiu, Y. Tang, J. Chen, R. Muriph, Z. Ye, C. Huang, J. Evans, E.P. Henske, Q. Xu, Lung-selective mRNA delivery of synthetic lipid nanoparticles for the treatment of pulmonary lymphangioleiomyomatosis, Proceedings of the National Academy of Sciences 119 (2022) e2116271119. https://doi.org/10.1073/pnas.2116271119.

[55] T. Nakamura, M. Kawai, Y. Sato, M. Maeki, M. Tokeshi, H. Harashima, The effect of size and charge of lipid nanoparticles prepared by microfluidic mixing on their lymph node transitivity and distribution, Mol Pharm 17 (2020) 944–953. https://doi.org/10.1021/acs.molpharmaceut.9b01182.

[56] J. Di, Z. Du, K. Wu, S. Jin, X. Wang, T. Li, Y. Xu, Biodistribution and non-linear gene expression of mRNA LNPs affected by delivery route and particle size, Pharm Res 39 (2022) 105–114. https://doi.org/10.1007/s11095-022-03166-5.

[57] N. Davies, D. Hovdal, N. Edmunds, P. Nordberg, A. Dahlén, A. Dabkowska, M.Y. Arteta, A. Radulescu, T. Kjellman, A. Höijer, F. Seeliger, E. Holmedal, E. Andihn, N. Bergenhem, A.-S. Sandinge, C. Johansson, L. Hultin, M. Johansson, J. Lindqvist, L. Björsson, Y. Jing, S. Bartesaghi, L. Lindfors, S. Andersson, Functionalized lipid

nanoparticles for subcutaneous administration of mRNA to achieve systemic exposures of a therapeutic protein, Mol Ther Nucleic Acids 24 (2021) 369–384. https://doi.org/10.1016/j.omtn.2021.03.008.

[58] N. Pardi, S. Tuyishime, H. Muramatsu, K. Kariko, B.L. Mui, Y.K. Tam, T.D. Madden, M.J. Hope, D. Weissman, Expression kinetics of nucleoside-modified mRNA delivered in lipid nanoparticles to mice by various routes, Journal of Controlled Release 217 (2015) 345–351. https://doi.org/10.1016/j.jconrel.2015.08.007.

[59] S. Ols, L. Yang, E.A. Thompson, P. Pushparaj, K. Tran, F. Liang, A. Lin, B. Eriksson, G.B. Karlsson Hedestam, R.T. Wyatt, K. Loré, Route of vaccine administration alters antigen trafficking but not innate or adaptive immunity, Cell Rep 30 (2020) 3964–3971. https://doi.org/10.1016/j.celrep.2020.02.111.

[60] M.A. Oberli, A.M. Reichmuth, J.R. Dorkin, M.J. Mitchell, O.S. Fenton, A. Jaklenec, D.G. Anderson, R. Langer, D. Blankschtein, Lipid nanoparticle assisted mRNA delivery for potent cancer immunotherapy, Nano Lett 17 (2017) 1326–1335. https://doi.org/10.1021/acs.nanolett.6b03329.

[61] F. Liang, G. Lindgren, A. Lin, E.A. Thompson, S. Ols, J. Röhss, S. John, K. Hassett, O. Yuzhakov, K. Bahl, L.A. Brito, H. Salter, G. Ciaramella, K. Loré, Efficient targeting and activation of antigen-presenting cells in vivo after modified mRNA vaccine administration in rhesus macaques, Molecular Therapy 25 (2017) 2635–2647. https://doi.org/10.1016/j.ymthe.2017.08.006.

[62] C. Jacoberger-Foissac, H. Saliba, M. Wantz, C. Seguin, V. Flacher, B. Frisch, B. Heurtault, S. Fournel, Liposomes as tunable platform to decipher the antitumor immune response triggered by TLR and NLR agonists, European Journal of Pharmaceutics and Biopharmaceutics 152 (2020) 348–357. https://doi.org/10.1016/j.ejpb.2020.05.026.

[63] M. Jayaraman, S.M. Ansell, B.L. Mui, Y.K. Tam, J. Chen, X. Du, D. Butler, L. Eltepu, S. Matsuda, J.K. Narayanannair, K.G. Rajeev, I.M. Hafez, A. Akinc, M.A. Maier, M.A. Tracy, P.R. Cullis, T.D. Madden, M. Manoharan, M.J. Hope, Maximizing the potency of siRNA lipid nanoparticles for hepatic gene silencing in vivo, Angewandte Chemie International Edition 51 (2012) 8529–8533. https://doi.org/10.1002/anie.201203263.

[64] S. Sabnis, E.S. Kumarasinghe, T. Salerno, C. Mihai, T. Ketova, J.J. Senn, A. Lynn, A. Bulychev, I. McFadyen, J. Chan, Ö. Almarsson, M.G. Stanton, K.E. Benenato, A novel Amino lipid series for mRNA delivery: Improved endosomal escape and sustained pharmacology and safety in non-human primates, Molecular Therapy 26 (2018) 1509–1519. https://doi.org/10.1016/j.ymthe.2018.03.010.

[65] R.J.T. Leboux, N. Benne, W.L. van Os, J. Bussmann, A. Kros, W. Jiskoot, B. Slütter, High-affinity antigen association to cationic liposomes via coiled coil-forming peptides induces a strong antigen-specific CD4+ T-cell response, European Journal of Pharmaceutics and Biopharmaceutics 158 (2021) 96–105. https://doi.org/10.1016/j.ejpb.2020.11.005.